


Comparative study of methods to estimate hydraulic parameters in the hydraulically undisturbed Opalinus Clay (Switzerland)

Catherine Yu^{1,2}  · Jean-Michel Matray¹ · Julio Gonçalves² · David Jaeggi³ · Werner Gräsle⁴ · Klaus Wiczorek⁵ · Tobias Vogt⁶ · Erik Sykes⁷

Received: 11 March 2016 / Accepted: 17 December 2016 / Published online: 25 February 2017
© The Author(s) 2017. This article is published with open access at Springerlink.com

Abstract The deep borehole (DB) experiment gave the opportunity to acquire hydraulic parameters in a hydraulically undisturbed zone of the Opalinus Clay at the Mont Terri rock laboratory (Switzerland). Three methods were used to estimate hydraulic conductivity and specific storage values of the Opalinus Clay formation and its bounding formations through the 248 m deep borehole BDB-1: application of a Poiseuille-type law involving petrophysical measurements, spectral analysis of pressure time series and in situ hydraulic tests. The hydraulic conductivity range in the Opalinus Clay given by the first method is 2×10^{-14} – $6 \times 10^{-13} \text{ m s}^{-1}$ for a cementation factor ranging between 2 and 3. These results show low

vertical variability whereas in situ hydraulic tests suggest higher values up to $7 \times 10^{-12} \text{ m s}^{-1}$. Core analysis provides economical estimates of the homogeneous matrix hydraulic properties but do not account for heterogeneities at larger scale such as potential tectonic conductive features. Specific storage values obtained by spectral analysis are consistent and in the order of 10^{-6} m^{-1} , while formulations using phase shift and gain between pore pressure signals were found to be inappropriate to evaluate hydraulic conductivity in the Opalinus Clay. The values obtained are globally in good agreement with the ones obtained previously at the rock laboratory.

Keywords Argillaceous formation · Hydraulic well tests · Poiseuille-type law · Harmonic tidal analysis · Hydraulic conductivity · Specific storage · Nuclear waste disposal

Editorial handling: P. Bossart and A. G. Milnes.

This is paper #4 in the Mont Terri Special Issue of the Swiss Journal of Geosciences (see Bossart et al. 2017, Table 3 and Fig. 7).

✉ Catherine Yu
catherine.jiyu@irsn.fr

- ¹ Institut de Radioprotection et de Sûreté Nucléaire, 31 Allée du Général Leclerc, 92260 Fontenay-aux-Roses, France
- ² Aix Marseille Université UMR 6635 CEREGE Technopôle Environnement Arbois-Méditerranée, BP80, 13545 Aix-en-Provence Cedex 4, France
- ³ Federal Office of Topography Swisstopo, Seftigenstrasse 264, 3084 Wabern, Switzerland
- ⁴ Federal Institute for Geosciences and Natural Resources (BGR), Stilleweg 2, 30655 Hannover, Germany
- ⁵ Global Research for Safety (GRS), Schwertnergasse 1, 50667 Cologne, Germany
- ⁶ National Cooperative for the Disposal of Radioactive Waste (Nagra), Hardstrasse 73, 5430 Wettingen, Switzerland
- ⁷ Nuclear Waste Management Organization, 22 St. Clair Ave. E., Toronto, ON, Canada

1 Introduction

Based on favourable confining properties, such as low permeability, strong retention and self-sealing capacities, clay formations are the preferred host rock option for a deep geological repository of long-lived, intermediate and high level radioactive waste in several countries including France, Belgium and Switzerland. In the latter country, the Opalinus Clay (OPA) has been selected as a potential host rock for a disposal facility (Nagra 2002) and has been studied at the Mont Terri rock laboratory since 1996. The laboratory is located at a depth of ca. 280 m, in the security gallery of the A16 Transjurane motorway, which crosses the Jura Mountains in north-western Switzerland.

The accurate hydraulic characterisation of low permeability formations is of high importance to ensure the safety of a geological repository. Hydraulic properties can be estimated by various laboratory and field experiments (Van

der Kamp 2001; Yu et al. 2013), including empirical methods based on the rock matrix properties (Chapuis and Aubertin 2003), falling head or constant head permeameter tests in laboratory (Boulin et al. 2012), and in situ field tests that rely on measurement of pore pressure or water level changes due to tidal natural loading (Bredehoeft 1967; Merritt 2004; Jiang et al. 2013) or artificial application of an hydraulic pressure different from the static formation pressure (Neuzil 1982; Butler 1998; Mejías et al. 2009). As these methods are carried out from sub-millimetre to hectometre investigation scales, scale dependency can affect the results (Keller et al. 1989; Neuzil 1994).

This paper compares three different techniques to estimate hydraulic properties of the Opalinus Clay: application of a Poiseuille-type law involving petrophysical measurements, in situ packer tests and spectral analysis of pore pressure time series.

2 Geological setting

The Opalinus Clay at the Mont Terri site is an overconsolidated claystone of Aalenian-Toarcian age, overlain by 800 m of Middle to Late Jurassic limestones, marls and shales, and underlain by 400 m of Early Jurassic to Triassic marls and limestones, dolomites and anhydrites (Fig. 1). The thickness

of the Opalinus Clay in the Mont Terri anticline varies between 130 m in the BDB-1 borehole and 160 m at rock laboratory level, depending on the tectonic contribution. This corresponds to a sedimentary thickness of about 120 m, when corrected for tectonic overthrusting. The Opalinus Clay reached a burial depth of 1350 m about 120 Ma ago during early Cretaceous, which resulted in a maximum temperature of 80–90 °C (Mazurek et al. 2006). A period of marine regression occurred between 100 and 40 Ma, leading to a subaerial exposure of the top of the Malm limestone. Starting about 40 Ma, the rifting of the Rhine Graben affected Northern Switzerland, resulting in considerable subsidence of the area in the mid-Tertiary, which brought the Opalinus Clay sequence back to about 500 m depth. Two sea invasions into the Mont Terri area took place during Priabonian (37–34 Ma) and during the Rupelian (34–28 Ma) (Clauer et al. 2017). Late Alpine folding during the late Miocene to Pliocene (about 12–3 Ma) formed the Folded Jura. Erosion exposed the core of the Mont Terri anticline towards 2.5 Ma, and allowed fresh water infiltration to the Middle Jurassic limestones. Similarly, infiltration to the Early Jurassic limestones would have started in the Quaternary, around 350 thousand years ago (Pearson et al. 2003).

Three main facies were identified within the Opalinus Clay (Blaesi et al. 1991): a shaly facies in the lower part of the sequence, a thin carbonate-rich sandy facies in the

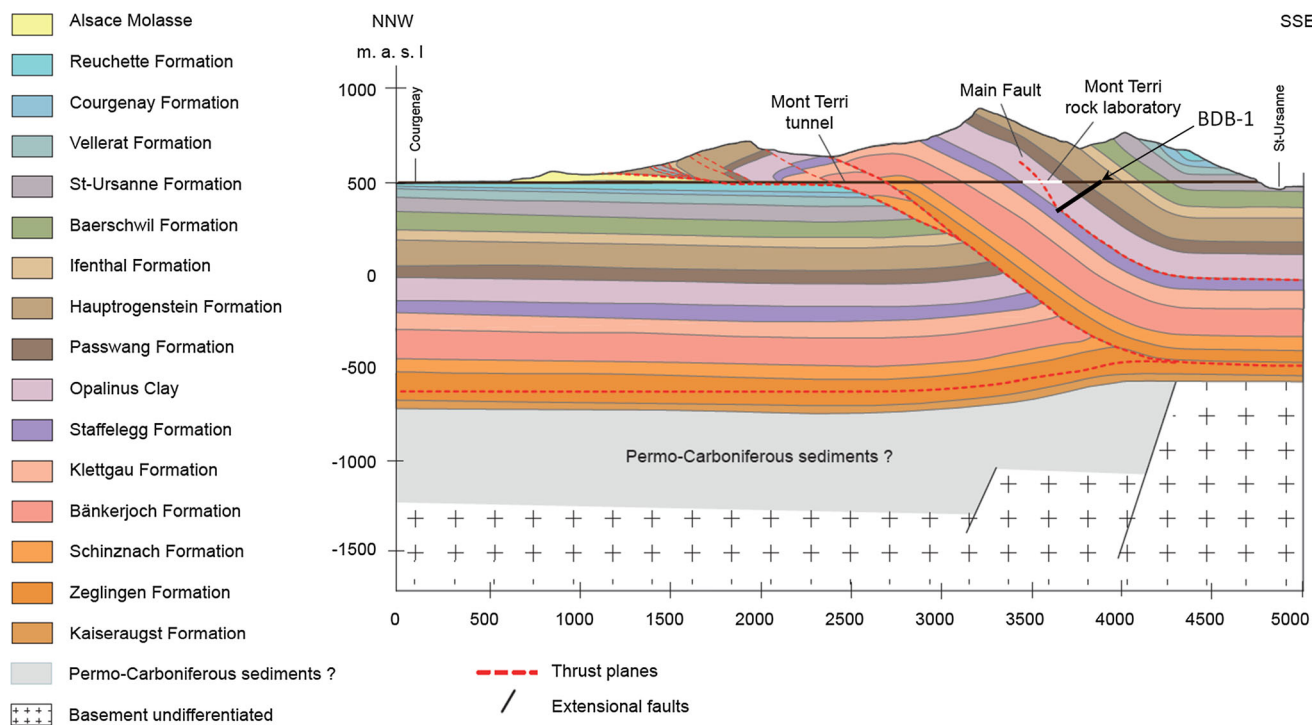


Fig. 1 Geological cross-section of the Mont Terri anticline. Location of the rock laboratory is indicated by a white line. The BDB-1 deep borehole, represented by a thick black line, crosses the lower part of

the Dogger aquifer, the entire Opalinus Clay formation and the upper part of the Liassic marls (adapted from Nussbaum et al. 2017)

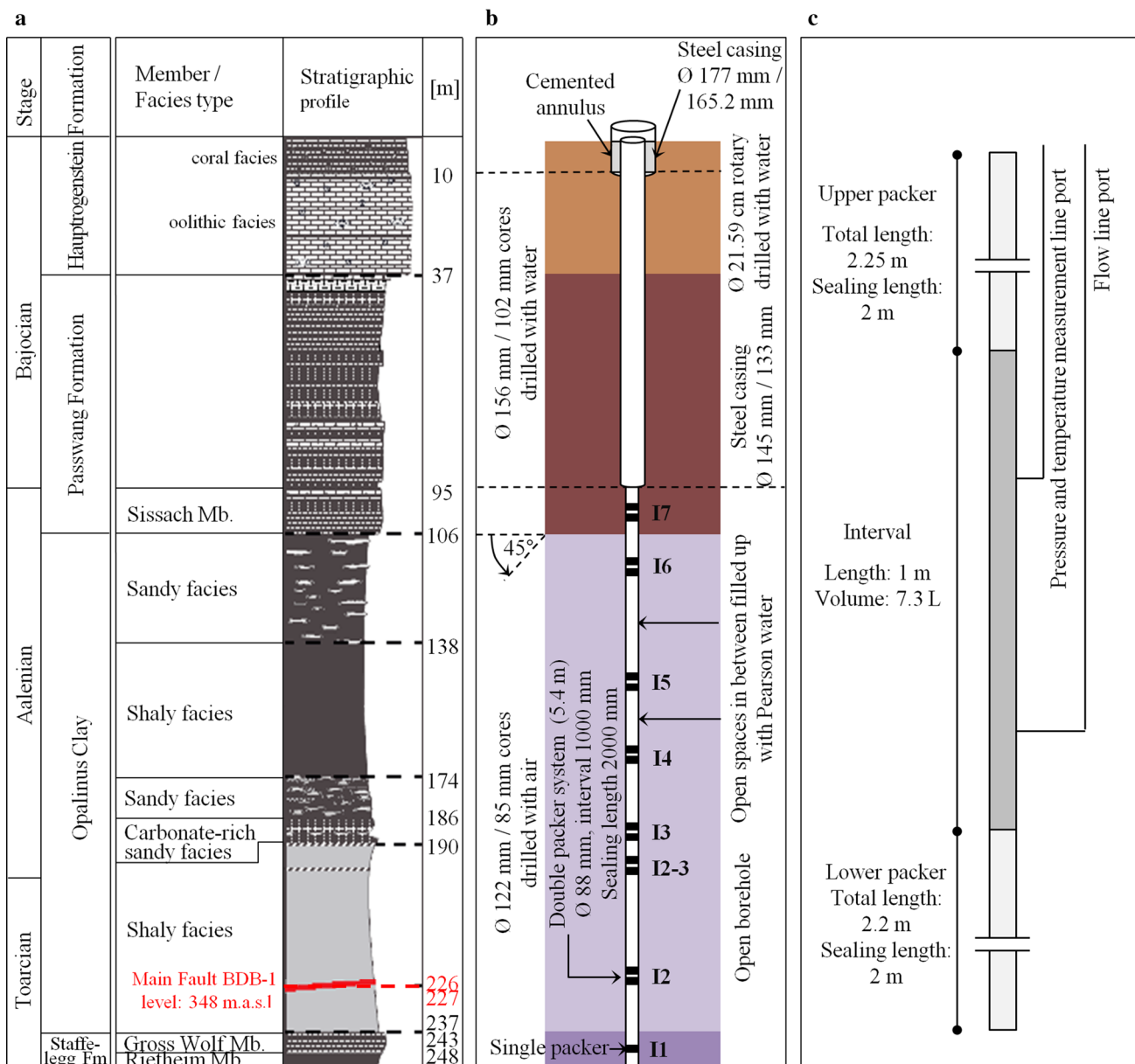


Fig. 2 a Stratigraphic sequence along the BDB-1 borehole; b BDB-1 borehole layout; c Layout of double packer elements (adapted from Hostettler et al. 2017)

middle part of the formation, and a sandy facies interstratified with shaly facies in the upper sequence. The shaly facies mineral composition includes 27–78% of clay minerals (illite, chlorite, kaolinite and illite–smectite mixed layers), 4–29% of carbonates, 10–32% of quartz, and accessory feldspars, pyrite and organic matter (Bossart and Thury 2008).

Several minor tectonic faults and a larger fault zone called “Main Fault” can be observed in the Opalinus Clay (Nussbaum et al. 2011). Nagra’s investigations in deep boreholes at Riniken, Weiach, Schafisheim and Benken revealed that the tectonically disturbed zones are hydraulically similar to the undeformed matrix (Johns et al.

1995; Gautschi 2001). Based on permeameter tests and in situ packer tests, hydraulic conductivity values in tectonically disturbed zones are in the range of 2×10^{-14} to $2 \times 10^{-12} \text{ m s}^{-1}$, and specific storage ranges from 2×10^{-7} to $1.7 \times 10^{-4} \text{ m}^{-1}$ (Marschall et al. 2005).

3 BDB-1 deep borehole

The deep borehole experiment (DB) aims at evaluating the hydrogeological properties and processes of undisturbed Opalinus Clay at the Mont Terri rock laboratory. For the

Table 1 Specifications of the pressure and temperature sensors installed in BDB-1 borehole

Sensor type	Temperature	Pore pressure
Model	IST AG PT1000	Keller AG PAA-33X
Validity range	-50 to 650 °C	0-50 bars (absolute)
Accuracy	± (0.15 + 0.002 T) °C	0.05% FS

first time in this laboratory, a 247.5 m long 45° downward inclined borehole has been drilled through the Opalinus Clay and the bounding formations. The stratigraphic sequence crossed by the borehole is presented in Fig. 2a and is described in detail in Hostettler et al. (2017). The borehole was entirely cored for stratigraphic, petrophysical, mineralogical and geochemical studies. The Opalinus Clay section was drilled with air as drilling fluid. Drilling was immediately followed by the installation of a multi-packer system (Fierz and Rösli 2014) consisting in five double packer measuring intervals and an interval port within the Opalinus Clay, a single packer in the Staffelegg Formation at the bottom of the borehole, and a further double packer interval isolating the lowermost zone of the Passwang Formation (Fig. 2b, c). Intervals were equipped with sensors that enable long term monitoring of pressure and temperature (Table 1). Pressure sensors are located at the surface and connected by stainless steel lines to the interval fluids, whereas temperature sensors are located downhole inside the intervals.

4 Techniques for hydraulic parameters evaluation

4.1 Petrophysical model

Assuming a plane-parallel geometry, the intrinsic permeability can be computed across an argillaceous formation using a semi-empirical Poiseuille-type law (Kostek et al. 1992; Pape et al. 1999; Tremosa 2010):

$$k = \frac{b^2}{3F}, \quad (1)$$

where k is the intrinsic permeability [m^2], b is the half-pore size [m] and F is the formation factor [-], which accounts for the tortuosity of the porous media and can be determined using the Archie's law (Archie 1942):

$$F = \omega^{-m}, \quad (2)$$

where ω is the porosity [-] and m is the cementation factor. The formation factor can also be related to diffusion parameters (Boving and Grathwohl 2001; Van Loon and Mibus 2015) or electrical properties (Archie 1942), following Eqs. (3) and (4):

$$F = \frac{D_w}{D_e}, \quad (3)$$

where D_w is the diffusion coefficient in pure water [$\text{m}^2 \text{s}^{-1}$] and D_e is the effective diffusion coefficient [$\text{m}^2 \text{s}^{-1}$].

$$F = \frac{R_0}{R_w}, \quad (4)$$

where R_0 is the rock resistivity [ohm m] saturated with a brine of resistivity R_w [ohm m].

The half-pore size can be computed from petrophysical parameters according to the following relation based on a mass balance equation (Neuzil 2000; Altinier 2006):

$$b = \frac{\omega}{(1 - \omega)\rho_s A_s}, \quad (5)$$

where b is the half-pore size [m], ω is the porosity [-], ρ_s is the grain density [g m^{-3}] and A_s is the specific surface area [$\text{m}^2 \text{g}^{-1}$].

Intrinsic permeability and hydraulic conductivity are linked according to:

$$K = \frac{k\rho_f g}{\mu_f}, \quad (6)$$

where K is the hydraulic conductivity [m s^{-1}], ρ_f is the fluid density [kg m^{-3}], g is the gravity acceleration [m s^{-2}] and μ_f is the fluid dynamic viscosity [Pa s].

Fluid dynamic viscosity was estimated according to Mercer et al. (1975):

$$\mu_f = (5.38 + 3.8A - 0.26A^2) \times 10^{-3}, \quad (7)$$

with

$$A = \frac{T - 150}{100}, \quad (8)$$

where μ_f is the fluid dynamic viscosity [Pa s] and T is the temperature [°C].

The Unesco equation of state (1981) was used to determine the fluid density as a function of salinity, temperature and pressure.

Determination of petrophysical parameters were performed in laboratory on representative element volume samples taken from the central part of BDB-1 drillcores. Porosity and water contents were determined by weighing before and after oven-drying at 105 °C until mass stabilisation. Density and degree of saturation were calculated based on Archimede's principle after sample immersion into kerdane following the experimental protocol first proposed by Monnier et al. (1973) and later adapted by Matray et al. (2007) for argillite samples. Grain density was evaluated using a helium pycnometer (Micromeritics® AccuPyc II 1340) on oven-dried samples and also recalculated from results of X-Ray diffraction measurements on bulk samples.

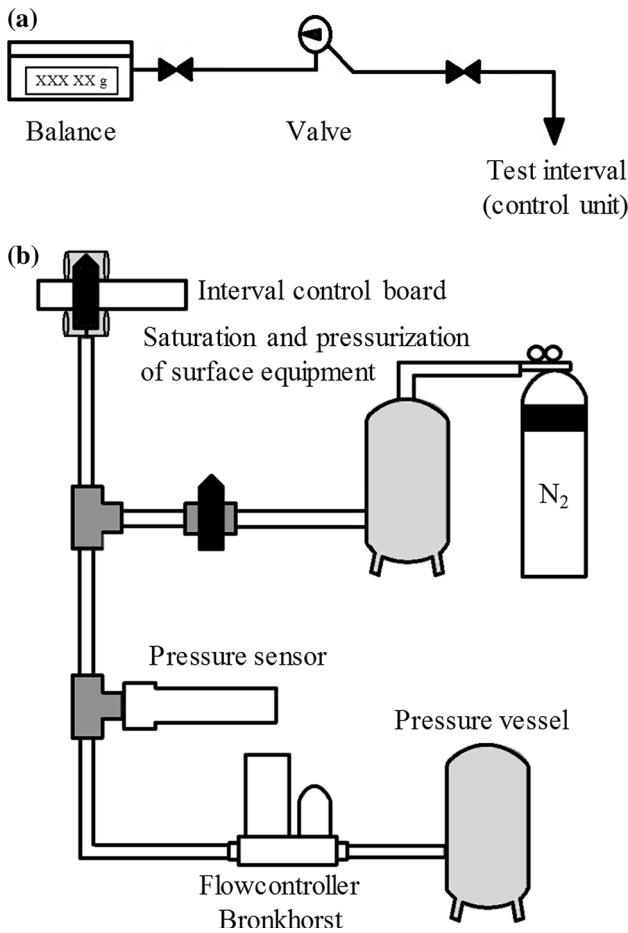


Fig. 3 Experimental set up for: **a** pulse withdrawal tests; **b** constant rate pumping tests performed on BDB-1 borehole (©Solexperts)

4.2 In-situ hydraulic testing experiments

Hydraulic in situ testing in boreholes, also referred as well testing, is the most common method used in groundwater and oil industries to acquire the hydraulic properties of geological formations. Pulse withdrawal tests and constant

rate withdrawal tests were conducted in BDB-1 borehole, from March 11th to November 16th 2015. During a withdrawal pulse test, pressure is lowered abruptly by opening and closing the downhole shut-in valve (Bredehoeft and Papadopoulos 1980; Neuzil 1982). These tests are preferred as initial phase because they give an immediate measurement of the system compressibility and generally require shorter time frame than pumping tests. Given its quick hydraulic response, performing more pulse tests on interval 1 (Staffellegg Formation, Fig. 2b) was possible, whereas two pulse tests were carried out on each of the other intervals.

Constant rate withdrawal test parameters such as flow rate and flow duration must be chosen with caution. In low permeability media, high flow rates can lead to desaturation of the measuring intervals and extreme drops in pressure. Therefore, a flowmeter able to sustain a very low pumping rate of 0.3 g h⁻¹ for several days (Bronkhorst® μ-flow L01) was used to test intervals 2 to 7 (Fig. 2b), for which the hydraulic responses to pulse testing were the slowest. Interval 1 was tested with a higher flow rate of 5 ml min⁻¹ using a Bronkhorst® Liqui-Flow L10. Experimental setups for both kind of tests and associated hydraulic responses are respectively reported in Figs. 3 and 4. Flowmeter failed during the testing of intervals 2 and 6 and approximately two months of pressure recovery were required before performing a second test on these test chambers.

Hydraulic test data were analysed using the well-test interpretation program nSIGHTS, which was developed by INTERA for Sandia National Laboratories (Beauheim and Roberts 2004). The code is based on Barker’s equation (1988), which describes flow in an n-dimensional space, and does not restrict to integer dimensions (Beauheim et al. 2004).

$$S_s \frac{\partial h}{\partial t} = \frac{K}{r^{n-1}} \frac{\partial}{\partial r} \left(r^{n-1} \frac{\partial h}{\partial r} \right), \quad (9)$$

where S_s is the specific storage coefficient [m⁻¹], h is the hydraulic head [m], t is the elapsed time [s], K is the

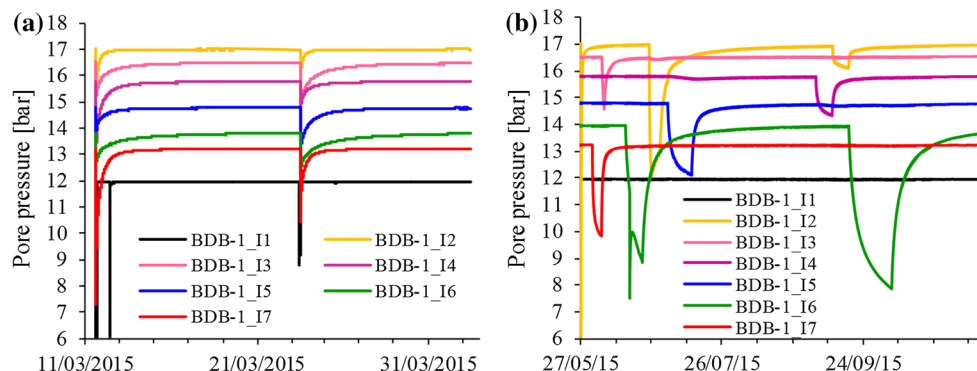


Fig. 4 Records of pore pressure responses in the seven intervals of BDB-1 borehole to: **a** pulse tests; **b** constant rate withdrawal tests

Table 2 Plausibility ranges set in nSIGHTS for fitted parameters

Fitted parameter	Plausibility range
K [m s ⁻¹]	
Interval 1	10 ⁻¹³ –10 ⁻⁸
Interval 2 to 7	10 ⁻¹³ –10 ⁻¹¹
S _s [m ⁻¹]	10 ⁻⁸ –10 ⁻⁴
Flow dimension [–]	1–3.5
Skin thickness [cm]	0.5–30
External boundary radius [m]	0–5

K stands for hydraulic conductivity and S_s for specific storage. Skin zone conductivity ranges were set one order of magnitude higher compared to intact rock

hydraulic conductivity [m s⁻¹], r is the radial distance from borehole [m], and n is the flow dimension [–].

The flow area is defined as

$$A(r) = b^{3-n} \frac{2\pi^{n/2}}{\Gamma^{n/2}} r^{n-1}, \quad (10)$$

where b is the extent of the flow zone [m], and Γ is the gamma function [–].

nSIGHTS is able to take account of borehole inclination by adjusting parameters such as formation thickness or capacitive effect. Equations are programmed as functions of pressure and the code uses unsensitively pressure or hydraulic head data according to user configuration. Flow is simulated in saturated conditions under a pressure gradient between the well and the external boundary of the model following Dupuit conditions. Density effects do not intervene directly in the equation system, as density is considered constant in the test interpretation.

Uncertainties associated with the fitted parameters are evaluated by performing random perturbation analyses. Plausibility ranges for fitted parameters were defined prior to the parameter optimisation procedure (Table 2). During the inverse parameter estimation, nSIGHTS provides best-fit results within these pre-defined ranges. Optimisation was performed using a simplex approach. Uncertainties associated with the fitted parameters are evaluated by performing random perturbation analyses (not detailed in this paper).

4.3 Tidal analysis on pore pressure time series

Rotational and gravitational forces exerted by the sun and the moon on the Earth induce latitudinal and longitudinal strains within the solid matrix and cause deformations with two dominant periods: diurnal and semi-diurnal. The tidal gravitational potential can be resolved into a finite set of tidal components described as harmonics, which are sinusoidal functions of given amplitude and frequency (Doodson and Warburg 1941; Cutillo and Bredehoeft

2011). Five main components account for about 95% of the tidal potential: the M₂ and N₂ semidiurnal lunar tides, the S₂ semidiurnal solar tide, the O₁ diurnal lunar tide, and the K₁ diurnal lunar-solar tide.

Seasonal or climatic variations, anthropogenic activities and tidal forces induce hydraulic pressure changes in geological formations. The amplitude of the pressure response depends on the poroelastic response of the aquifer matrix. Pressure signal can therefore be analysed to determine hydrogeological properties, such as specific storage, effective porosity and hydraulic conductivity. The models used in this work are based on Terzaghi's (1936) effective stress concept, which assumes a constant total stress distributed between grains and fluid stress. Bredehoeft (1967) related tidal strain to specific storage:

$$S_s = \frac{|\Delta\varepsilon|}{|\Delta h|}, \quad (11)$$

where S_s is the specific storage [m⁻¹], $|\Delta\varepsilon|$ is the amplitude of volumetric strain fluctuation fixed at 2×10^{-8} for the M₂ tide (Melchior 1978), and $|\Delta h|$ is the amplitude of relative pressure head fluctuations [m].

Jacob's (1940) formula was used to compute the porosity:

$$\omega = \frac{E_W S_s B}{\rho_f g}, \quad (12)$$

where ω correspond to the porosity [–], E_W is the stiffness modulus of water, equal to 2.05 GPa, S_s is the specific storage [m⁻¹], B is the barometric efficiency [–], which reflects the elastic response of the system, ρ_f is the fluid density, and g is the gravity acceleration equal to 9.81 m s⁻².

Hydraulic conductivity was estimated with formulations using the M₂ harmonic amplitude and phase shift (Boldt-Leppin and Hendry 2003; Timms and Acworth 2005), measured at two depths, z_1 and z_2 [m]:

$$K_v^{Amp}(f_{M_2}) = S_s(f_{M_2}) \frac{(z_1 - z_2)^2}{(f_{M_2})^{-1}} \left[\ln \left(\frac{A_{z_1}(f_{M_2})}{A_{z_2}(f_{M_2})} \right) \right]^{-2} \quad (13)$$

$$K_v^{Amp}(f_{M_2}) = S_s(f_{M_2}) \frac{(z_1 - z_2)^2}{(f_{M_2})^{-1}} \left[\ln \left(\frac{A_{z_1}(f_{M_2})}{A_{z_2}(f_{M_2})} \right) \right]^{-2}, \quad (14)$$

where K_v^{Amp} is the “amplitude effective hydraulic conductivity”, A_{z_1} and A_{z_2} [kPa], are the M₂ earth tide amplitude associated to the sensors, S_s [m⁻¹] is the arithmetic mean of the effective specific storage coefficients obtained individually for the two sensors, f_{M_2} [s⁻¹] is the frequency of the M₂ earth tide equal to 2.236×10^{-5} Hz, $K_v^{\Delta\varphi}$ [m s⁻¹] is the “phase effective hydraulic conductivity”, and $\Delta\varphi$ [rad] is the spectral phase shift between the sensors.

Spectral analysis of BDB-1 borehole pressure dataset was performed using the Multi-Statistical Analysis Tool (MuSTAT v1), jointly developed by the Institut de

Radioprotection et de Sûreté Nucléaire and the Institut National Polytechnique de Toulouse (Fatmi et al. 2008; Ababou et al. 2012; Bailly et al. 2014). Consisting in a Python code associated with toolboxes programmed in Matlab, the package provides automatic features: (a) pre-processing of time series, that enables the detection of time gaps and spurious values, as well as data reconstruction by autoregressive first order process; (b) processing of a single time series; (c) cross-analysis of two time series.

5 Results at various scales of investigation

5.1 Sub-millimeter to centimeter scale

5.1.1 Petrophysical parameters

The petrophysical parameters necessary for the computation of intrinsic permeability are presented in Fig. 5 as a function of distance along BDB-1 borehole.

The mean water accessible porosity is 13.0% in the Opalinus Clay, with a lower average porosity of 12.0% in the sandy facies compared to the shaly facies, which exhibit a mean porosity of 13.5%. These values are lower than the mean value of 18% suggested by previous studies performed at the Mont Terri tunnel level. The Passwang

Formation presents slightly lower porosity values ranging between 8.1 and 14.6% with a mean value of 12.2%. The Hauptrogenstein is characterised by the lowest porosity with a mean value of 3.9%.

Grain densities obtained by helium pycnometry have a mean value of 2.74 g cm^{-3} in the Opalinus Clay overlying formations and of 2.72 g cm^{-3} in the argillaceous layer. The lowest grain densities are found in the bituminous Rietheim Member of the Staffelegg Formation (see Fig. 1a), ranging between 2.3 and 2.4 g cm^{-3} . These low values are probably linked to the presence of organic matter.

The Passwang Formation, which directly overlays the Opalinus Clay, does not reveal clear petrophysical discrepancies with the clay formation except for the specific surface area. This parameter has an average value of $13 \text{ m}^2 \text{ g}^{-1}$ in the carbonated section of the borehole and shows significant fluctuations linked to the marly composition of the Passwang Formation. A higher mean value of $29 \text{ m}^2 \text{ g}^{-1}$ characterises the Opalinus Clay.

The Opalinus Clay is also characterised by a low pore size. Analyses of nitrogen adsorption and desorption isotherms show that 70 to 93% of the connected porous network is constituted of mesopores (pore diameter between 2 and 50 nm), with a mean size of 13 nm. Calculation of the half-pore size from petrophysical parameters, following

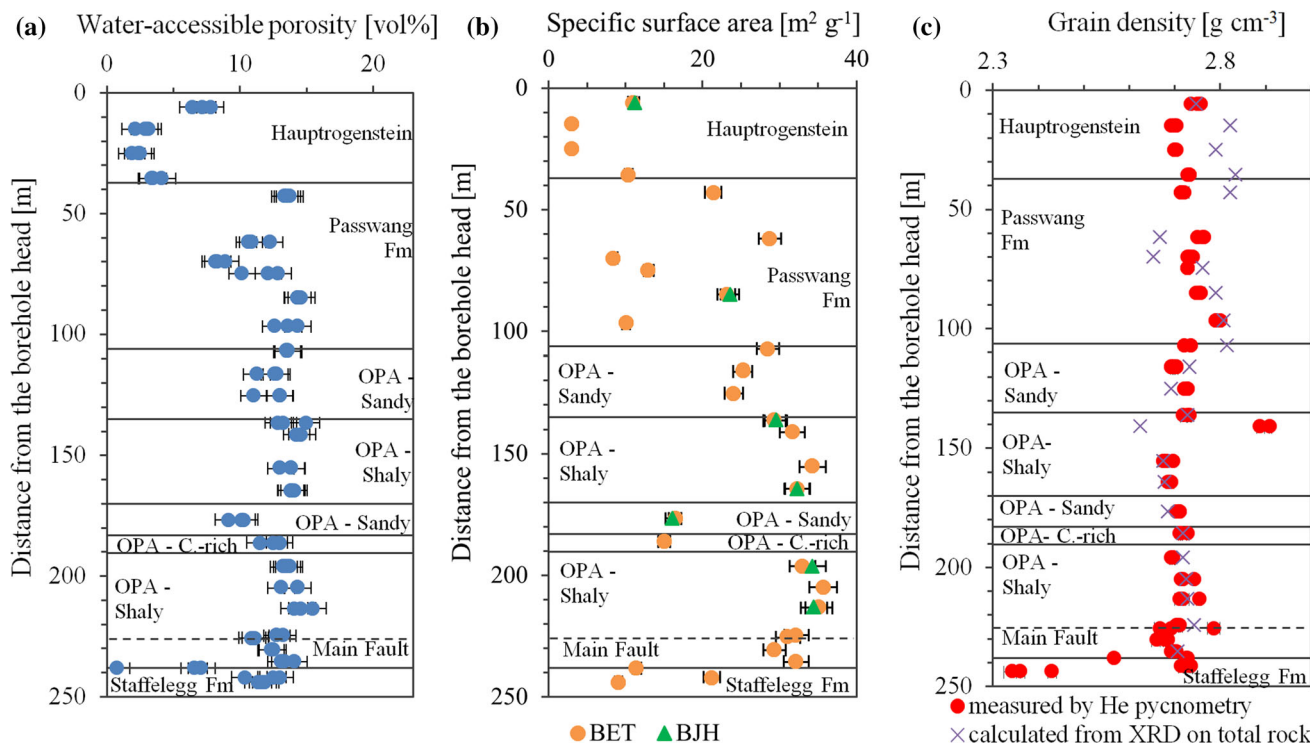


Fig. 5 Petrophysical parameters acquired along BDB-1 borehole: **a** Water accessible porosity acquired by oven-drying at 105 °C; **b** Specific surface area obtained by BJH and BET methods; **c** Grain density estimated by helium pycnometry on oven dried samples

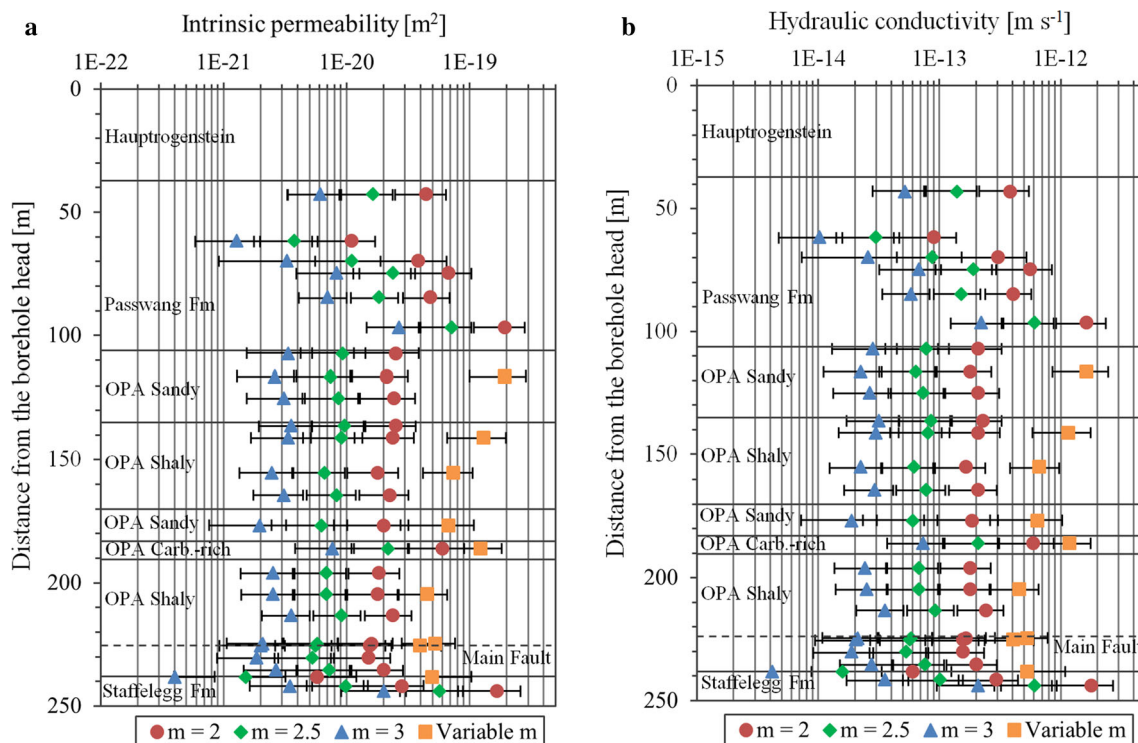


Fig. 6 **a** Intrinsic permeability profile and **b** hydraulic conductivity profile computed across the Opalinus Clay (OPA) and the Passwang Formation for cementation factor (m) of 2, 2.5 and 3. *Square symbols*

Eq. (5), gives mean pore sizes in the range of 3.1 to 7.3 nm.

Ranging between 1.3 and 5.4 (Horseman et al. 1996), the cementation factor was estimated to be close to 2 for compacted and deeply buried sediments (Ullman and Aller 1982; Tremosa 2010). Van Loon et al. (2003) related the effective diffusion coefficient of tritium measured in the Opalinus Clay to its porosity using a cementation factor of 2.5. An attempt was made to compute cementation factors from conductivity values obtained by borehole logging in BDB-1 and water-accessible porosity determined at laboratory scale. No real conductivity of formation fluid was acquired in the Opalinus Clay, as this part of the borehole was drilled with air. Therefore, fluid conductivity values were estimated based on chlorinity data acquired on BDB-1 core samples (not detailed in this paper). Low values of cementation factors are thus obtained and range between 0.9 and 1.7.

5.1.2 Intrinsic permeability and hydraulic conductivity

The intrinsic permeability profiles (Fig. 6a) show a low vertical variability through the Opalinus Clay, where it ranges between 1.8×10^{-21} and 6.1×10^{-20} m² if a cementation factor varying between 2 and 3 is taken. For a

represent values for variable m computed based on conductivity logging measurements across the Opalinus Clay

cementation factor of 2.5, the mean intrinsic permeability is 7.7×10^{-21} m² for the Opalinus Clay shaly facies and 7.9×10^{-21} m² for its sandy facies. These values are in good agreement with the range of 1×10^{-21} and 6×10^{-20} m² obtained by gas injection experiments performed at the Mont Terri laboratory (Marschall et al. 2005). Based on the same cementation factor, difference can be seen in the carbonate-rich sandy facies, where values are about three times higher than in the shaly and the sandy facies. With a higher exponent $m = 3$, the resulting intrinsic permeability has a mean value of 7.6×10^{-21} m² and no clear distinction arises between the different facies. The intrinsic permeability values computed in the Passwang Formation and the Staffelegg Formation are much more heterogeneous and vary between 1.5×10^{-21} and 5.8×10^{-20} m².

The corresponding hydraulic conductivity profiles are presented in Fig. 6b and show similar trends compared with the intrinsic permeability profiles. The hydraulic conductivity obtained for the Opalinus Clay ranges between 1.9×10^{-14} and 5.8×10^{-13} m s⁻¹ for a cementation factor varying between 2 and 3. For a cementation factor of 2.5, the formation is characterised by a mean hydraulic conductivity of 8.3×10^{-14} m s⁻¹. No clear discrepancy between the shaly facies and the sandy

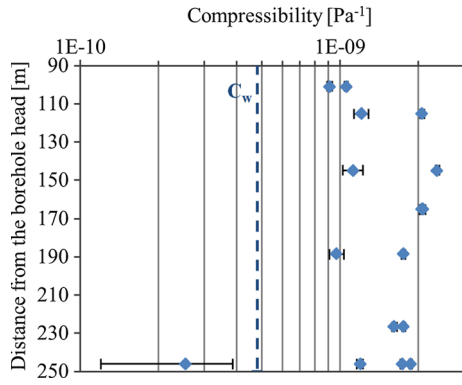


Fig. 7 System compressibility computed from pulse testing in BDB-1 borehole. *Dashed line* represents the water compressibility at 10 °C. The outlier in the *lower* part of the borehole is due to a very low withdrawn volume

facies is revealed, with respective mean values of 7.3×10^{-14} and $6.9 \times 10^{-14} \text{ m s}^{-1}$. These values are consistent with the range of 2×10^{-14} – $1 \times 10^{-12} \text{ m s}^{-1}$ reported in previous studies (Bossart and Thury 2008). The Passwang Formation and the Staffelegg Formation present a various range of hydraulic conductivities between 1.6×10^{-14} and $6.1 \times 10^{-13} \text{ m s}^{-1}$.

The computation of intrinsic permeability using variable cementation factors in the Opalinus Clay gives higher values in the range of 4.0×10^{-20} to $1.9 \times 10^{-19} \text{ m}^2$, corresponding to hydraulic conductivity values in the range of 4.1×10^{-13} – $1.7 \times 10^{-12} \text{ m s}^{-1}$.

5.2 Decimeter to meter scale: in situ hydraulic tests results

Pore pressure should be fully recovered from artificial disturbance induced by the installation procedure (e.g., drilling, logging, equipment installation) before starting a hydraulic test. Steady state was considered to be reached when the tidal components were detected on all pore pressure time series acquired in BDB-1 borehole, which indicate that the system is fully pressurised and saturated (see Sect. 5.3.1).

The observed compressibility of the test zone (C_{tz}) was deduced from pulse tests and computed according to:

$$C_{tz} = \frac{1}{V_{tz}} \frac{dV}{dP}, \quad (14)$$

where $V_{tz} [\text{m}^3]$ is the shut-in volume, $dV [\text{m}^3]$ is the withdrawn volume and $dP [\text{Pa}]$ is the pressure variation. Test zone compressibility in BDB-1 borehole varies 9.1×10^{-10} and $2.4 \times 10^{-9} \text{ Pa}^{-1}$ (Fig. 7), approximately up to a factor of 5 larger than water compressibility, which is equal to $4.8 \times 10^{-10} \text{ Pa}^{-1}$ at 10 °C (Kell 1975). The

discrepancy can be attributed to the mechanical compliance of the equipment.

Semi-logarithmic plots presented in Fig. 8 give a qualitative comparison of the hydraulic behaviours characterising the different tested intervals. Degree of pore pressure dissipation (U) and normalised drawdown pressure (U_{norm}) are respectively defined by the following equations:

$$U = \frac{U_t - U_0}{U_{min} - U_0} \quad (15)$$

$$U_{norm} = \frac{U_t - U_{min}}{U_0 - U_{min}}, \quad (16)$$

where U_t [kPa] is the pore pressure at time t , U_0 [kPa] is the hydrostatic pore pressure in situ and U_{min} [kPa] is the pore pressure reached after pulse application or at the end of the pumping phase.

Discrepancies in the degree of dissipation can be observed between tests performed on a same interval (Fig. 8a). Constant rate withdrawal tests were carried out using the same flow rate of 0.3 g h^{-1} for different durations. To compare the evolution of pore pressures in the measuring intervals during pumping phase, P_{min} was taken to correspond to the shortest pumping duration in the calculation of U_{norm} . If specific storage is assumed homogeneous through the Opalinus Clay, the order from left to right on Fig. 8b gives an indication of decreasing permeability.

The application of a composite model, which takes into account a damaged skin zone, was required for most of the test numerical interpretations. Taking as an example the first pulse test carried out on BDB-1 Interval 2, Fig. 9 shows a comparison of the residuals (measured value minus simulated value) to that of a normal distribution, using a homogeneous model and a composite one. The homogeneous model appears to be unsatisfactory because the residuals are not normally distributed, which indicates the presence of a systematic error.

Pulse tests and constant rate pumping tests results are respectively compiled in Table 3. Pulse testing revealed the highest hydraulic conductivity values in the Staffelegg Formation (Interval 1, see Fig. 2b) with best fit values ranging from 2.1×10^{-10} to $5.9 \times 10^{-10} \text{ m s}^{-1}$. Located in the basal shaly facies of Opalinus Clay (Interval 2), the bottom part of the main fault zone is characterised by conductivity values from 3.1×10^{-12} to $7.3 \times 10^{-12} \text{ m s}^{-1}$ and do not differ from the upper shaly facies represented by Interval 4 and 5 (Fig. 10), whose best estimates are up to $4.2 \times 10^{-12} \text{ m s}^{-1}$. The lowest values are found in the sandy facies (Interval 6, best fit values up to $2.7 \times 10^{-13} \text{ m s}^{-1}$), and the carbonate-rich sandy facies (Interval 3, best fit values up to $5.1 \times 10^{-13} \text{ m s}^{-1}$). The basal part of the Passwang

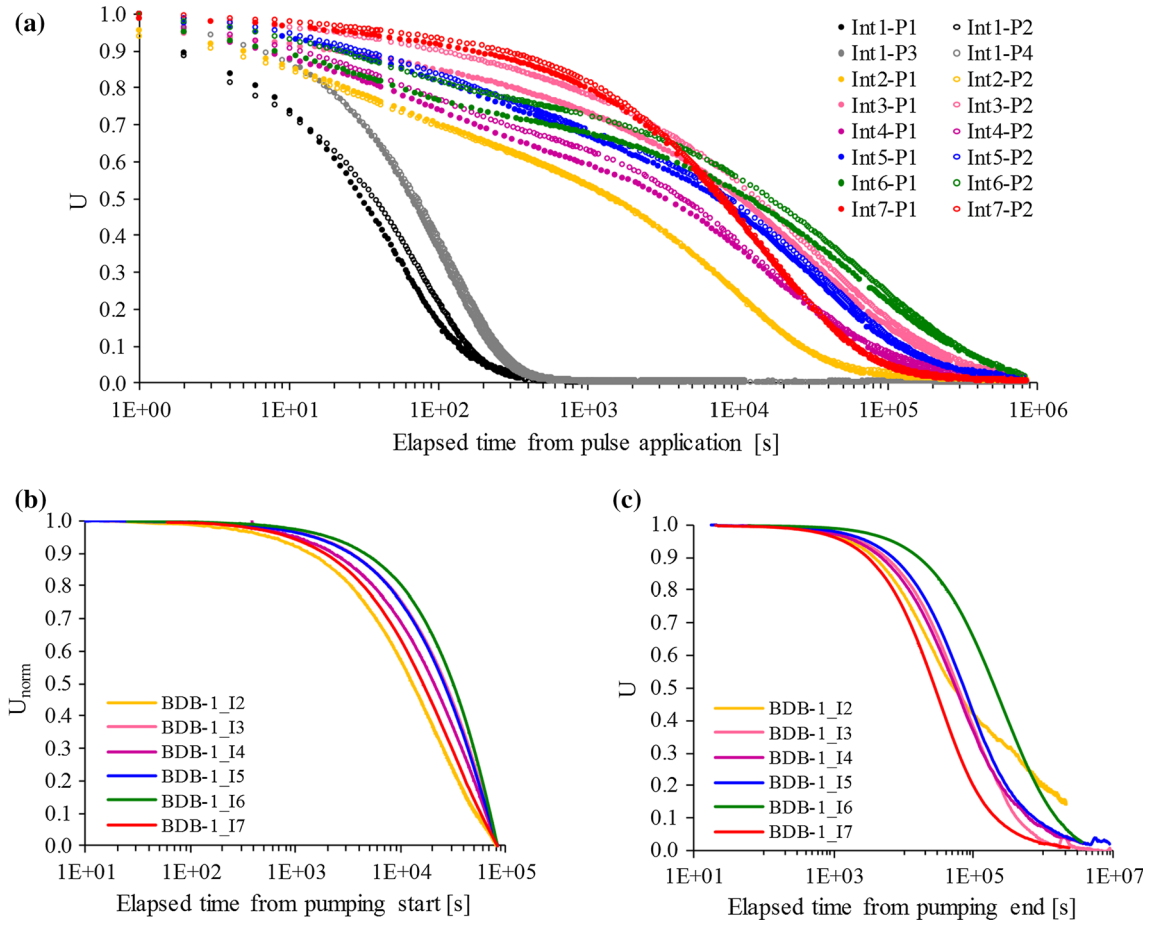


Fig. 8 Comparison of the different tests performed on BDB-1 borehole: **a** degree of dissipation associated to the recovery phases of pulse withdrawal tests; **b** normalised pressure drawdown during

constant rate withdrawal tests and **c** degree of dissipation following the end of the withdrawal phase

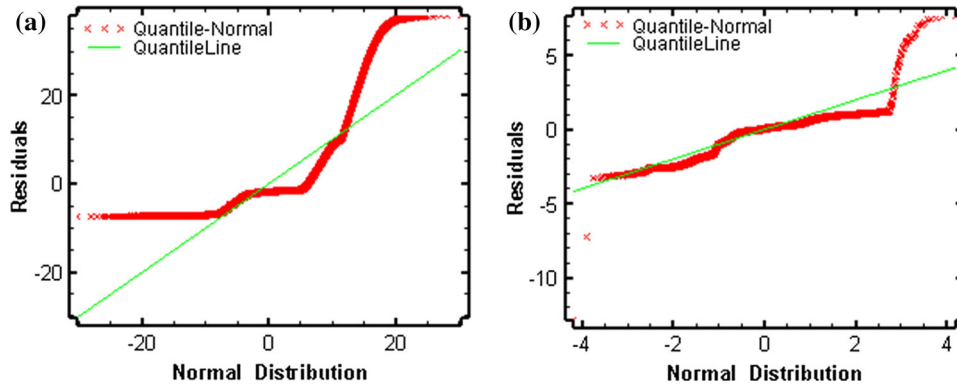


Fig. 9 Example of residual plots for the optimization of Interval 2 (Opalinus Clay shaly facies) pulse sequence fit to the Cartesian pressure response using **a** an homogeneous model and **b** a composite model with skin

Formation, represented by Interval 7, shows similar hydraulic conductivity values to Opalinus Clay (5.8×10^{-13} – 1.4×10^{-12} m s⁻¹).

The analyses results of the constant flowrate withdrawal tests are quite consistent with those obtained from pulse tests. Indeed, a similar trend can be observed with slightly

Table 3 Parameter estimates from BDB-1 borehole pulse withdrawal tests and constant rate (CR) withdrawal tests (K [m s⁻¹]: hydraulic conductivity; S_s [m⁻¹]: specific storage; n: flow dimension; t_s [cm]: skin thickness)

Test	Interval	T _s [cm]	K [m s ⁻¹]			S _s [m ⁻¹]			n	
			Formation		Skin	Formation		Skin	Range	Best fit
			Range	Best fit	Best fit	Range	Best fit	Best fit		
Pulse										
C1-1	I ₁	-	1 × 10 ⁻¹⁰ -3.5 × 10 ⁻¹⁰	2.1 × 10 ⁻¹⁰	-	6 × 10 ⁻⁹ - 6.3 × 10 ⁻⁸	1.4 × 10 ⁻⁸	-	1.9-2.7	2.2
C1-2	I ₁	-	1 × 10 ⁻¹¹ -1 × 10 ⁻⁷	4.2 × 10 ⁻¹⁰	-		1.4 × 10 ⁻⁶	-		2.0
C1-3	I ₁	-	1 × 10 ⁻¹¹ -1 × 10 ⁻⁷	5.6 × 10 ⁻¹⁰	-		6.3 × 10 ⁻⁸	-		2.4
C1-6	I ₁	-	3 × 10 ⁻¹¹ -1 × 10 ⁻⁸	5.9 × 10 ⁻⁹	-		8.3 × 10 ⁻⁷	-		2.0
C2-1	I ₂	0.5	2 × 10 ⁻¹² -3 × 10 ⁻¹¹	3.1 × 10 ⁻¹²	7.8 × 10 ⁻¹²	1 × 10 ⁻⁷ - 3 × 10 ⁻⁵	5.2 × 10 ⁻⁶	4.3 × 10 ⁻⁵	1.8-3.0	2.8
C2-2	I ₂	0.5	2 × 10 ⁻¹² -1 × 10 ⁻¹⁰	7.3 × 10 ⁻¹²	1.0 × 10 ⁻¹¹	1 × 10 ⁻⁷ - 2 × 10 ⁻⁵	3.0 × 10 ⁻⁶	4.7 × 10 ⁻⁵	1.4-2.9	2.0
C3-1	I ₃	0.5	1 × 10 ⁻¹³ -3 × 10 ⁻¹²	5.1 × 10 ⁻¹³	1.6 × 10 ⁻¹²	5 × 10 ⁻⁷ - 3 × 10 ⁻⁵	3.7 × 10 ⁻⁶	1.2 × 10 ⁻⁵	1.4-3.1	2.1
C3-2	I ₃	0.5	2 × 10 ⁻¹³ -2 × 10 ⁻¹²	4.9 × 10 ⁻¹³	1.6 × 10 ⁻¹²	2 × 10 ⁻⁶ - 3 × 10 ⁻⁵	1.1 × 10 ⁻⁵	1.5 × 10 ⁻⁵	1.4-3.4	2.5
C4-1	I ₄	0.5	1 × 10 ⁻¹² -9 × 10 ⁻¹²	2.3 × 10 ⁻¹²	5.7 × 10 ⁻¹²	2 × 10 ⁻⁶ - 1 × 10 ⁻⁵	6.4 × 10 ⁻⁶	5.5 × 10 ⁻⁵	1.7-3	2.3
C4-2	I ₄	2.0	7 × 10 ⁻¹³ -1 × 10 ⁻¹¹	4.2 × 10 ⁻¹²	2.7 × 10 ⁻¹¹	1 × 10 ⁻⁶ - 2 × 10 ⁻⁵	2.2 × 10 ⁻⁶	9.7 × 10 ⁻⁶	1.5-3	2.0
C5-1	I ₅	0.5	4 × 10 ⁻¹³ -4 × 10 ⁻¹²	1.6 × 10 ⁻¹²	1.4 × 10 ⁻¹²	3 × 10 ⁻⁷ - 8 × 10 ⁻⁶	1.0 × 10 ⁻⁶	2.6 × 10 ⁻⁵	1.8-2.9	1.9
C5-2	I ₅	0.5	4 × 10 ⁻¹³ -3 × 10 ⁻¹²	1.0 × 10 ⁻¹²	2.7 × 10 ⁻¹²	1 × 10 ⁻⁶ - 3 × 10 ⁻⁵	8.5 × 10 ⁻⁶	4.7 × 10 ⁻⁵	1-3	2.5
C6-1	I ₆	1.5	8 × 10 ⁻¹⁴ -8 × 10 ⁻¹³	1.9 × 10 ⁻¹³	1.4 × 10 ⁻¹¹	8 × 10 ⁻⁷ - 1 × 10 ⁻⁵	6.6 × 10 ⁻⁶	6.6 × 10 ⁻⁶	1.7-3	2.6
C6-2	I ₆	0.5	2 × 10 ⁻¹³ -6 × 10 ⁻¹³	2.7 × 10 ⁻¹³	5.4 × 10 ⁻¹²	1 × 10 ⁻⁶ - 2 × 10 ⁻⁵	1.7 × 10 ⁻⁵	2.9 × 10 ⁻⁵	1.7-3	2.8
C7-1	I ₇	0.5	3 × 10 ⁻¹³ -4.5 × 10 ⁻¹²	5.8 × 10 ⁻¹³	3.7 × 10 ⁻¹³	4 × 10 ⁻⁷ - 2 × 10 ⁻⁵	3.7 × 10 ⁻⁶	1.9 × 10 ⁻⁶	1.9-3.5	3.0
C7-2	I ₇	0.5	4 × 10 ⁻¹³ -2 × 10 ⁻¹²	1.4 × 10 ⁻¹²	8.6 × 10 ⁻¹²	10 ⁻⁹ - 2 × 10 ⁻⁵	1.2 × 10 ⁻⁶	9.4 × 10 ⁻⁷	2.1-2.6	2.3
CR										
C1-7	I ₁	4.3	1 × 10 ⁻¹⁰ -1 × 10 ⁻⁹	5.0 × 10 ⁻¹⁰	5.7 × 10 ⁻⁹	1 × 10 ⁻⁸ - 1 × 10 ⁻⁴	8.2 × 10 ⁻⁶	6.2 × 10 ⁻⁵	2.0-3.0	2.1
C2-2	I ₂	14.2	4 × 10 ⁻¹³ -8 × 10 ⁻¹¹	3.9 × 10 ⁻¹²	3.5 × 10 ⁻¹¹		1.2 × 10 ⁻⁶	9.0 × 10 ⁻⁵	1.4-2.7	1.95
C3-3	I ₃	0.7	1 × 10 ⁻¹³ -2 × 10 ⁻¹²	9.9 × 10 ⁻¹³	1.6 × 10 ⁻¹²	3 × 10 ⁻⁸ - 6 × 10 ⁻⁵	1.5 × 10 ⁻⁵	4.9 × 10 ⁻⁵	1.5-3.0	1.9
C4-3	I ₄	1.4	4 × 10 ⁻¹⁴ -5 × 10 ⁻¹²	2.4 × 10 ⁻¹²	3.0 × 10 ⁻¹²	4 × 10 ⁻⁸ - 3 × 10 ⁻⁴	1.2 × 10 ⁻⁵	4.0 × 10 ⁻⁵	1.9-3.0	2.1
C5-3	I ₅	1.8	7 × 10 ⁻¹⁴ -9 × 10 ⁻¹²	8.1 × 10 ⁻¹³	1.5 × 10 ⁻¹¹	1 × 10 ⁻⁷ - 3 × 10 ⁻⁵	8.9 × 10 ⁻⁵	2.4 × 10 ⁻⁵	1.9-3.0	2.3
C6-3	I ₆	0.5	1 × 10 ⁻¹⁴ -4 × 10 ⁻¹²	2.2 × 10 ⁻¹³	1.1 × 10 ⁻¹²	1 × 10 ⁻⁷ - 2 × 10 ⁻⁵	7.7 × 10 ⁻⁶	9.9 × 10 ⁻⁵	1.5-2.9	2.5
C7-3	I ₇	0.6	1 × 10 ⁻¹³ -1 × 10 ⁻¹²	4.4 × 10 ⁻¹³	8.2 × 10 ⁻¹³	3 × 10 ⁻⁸ - 4 × 10 ⁻⁶	8.5 × 10 ⁻⁶	2.3 × 10 ⁻⁵	2.1-3.0	2.7

Shaded cells represent unrealistically wide range of uncertainties

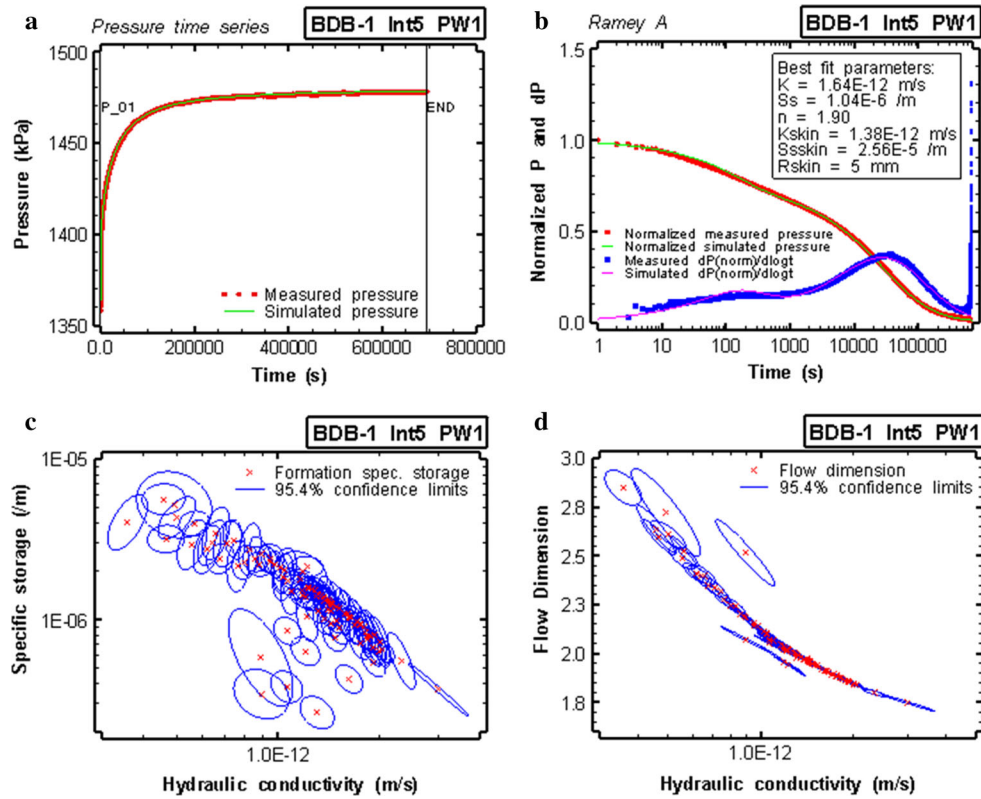


Fig. 10 a Simulation of a pulse test performed on BDB-1 Interval 5 located in the upper shaly facies of Opalinus Clay and b associated Ramey A plot with best fit parameters. Results of 200 perturbation analyses and their confidence regions (c and d)

higher permeability values in the shaly facies than in the sandy facies of Opalinus Clay.

Specific storage and flow dimension estimates are highly variable. One issue with single well hydraulic testing is that the volume of tested rock is limited to the immediate vicinity of the well.

5.3 Hectometer scale: tidal analysis

5.3.1 Tidal identification in BDB-1 pore pressure series

Detection of tidal components was performed on the pore pressure time series monitored by the sensors placed in BDB-1 borehole, with an acquisition time step set at 15 min. The four largest amplitude tidal components, O_1 , K_1 , S_2 and M_2 appear on all processed signals at the exact expected frequencies for time series between September 1st 2014 and March 10th 2015 (Fig. 11).

The form ratio is defined as the sum of the two main diurnal component amplitudes, K_1 and O_1 , divided by the sum of the two main semi-diurnal component amplitudes, M_2 and S_2 (Wiegel 1964). Tidal deformation through the Opalinus Clay at Mont Terri is characterised by a form ratio varying between 0.84 and 1.04, which indicates a

Fig. 11 Estimated Root Mean Square spectrum of pore pressure time series measured in BDB-1 borehole between 01/09/2014 and 10/03/2015. The following tides are observable: principal lunar semi-diurnal tide M_2 (2.236×10^{-5} Hz) and solar semi-diurnal tide S_2 (2.315×10^{-5} Hz), lunar diurnal tides K_1 (1.161×10^{-5} Hz) and O_1 (1.076×10^{-5} Hz), and the solar diurnal components S_1 (1.157×10^{-5} Hz) and P_1 (1.154×10^{-5} Hz)

mixed, mainly semi-diurnal tide (Table 4). The maximum value is found in the interval located in the Passwang Formation, for which the diurnal components have slightly higher amplitudes than the semi-diurnal ones. Except for this interval, the M_2 tide presents the highest amplitude among the four major tides.

5.3.2 Hydraulic parameters computation

The results of specific storage coefficient computation are given in Table 5. Specific storage values are ranging between 1.1×10^{-6} and $1.6 \times 10^{-6} \text{ m}^{-1}$ in the Opalinus Clay and are higher for the adjacent formations ($2.4 \times 10^{-6} \text{ m}^{-1}$ for the Lower Dogger limestone and $3.1 \times 10^{-6} \text{ m}^{-1}$ for the Staffelegg Formation). These estimates are consistent with the range given in the literature, deduced from in situ packer tests and permeameter

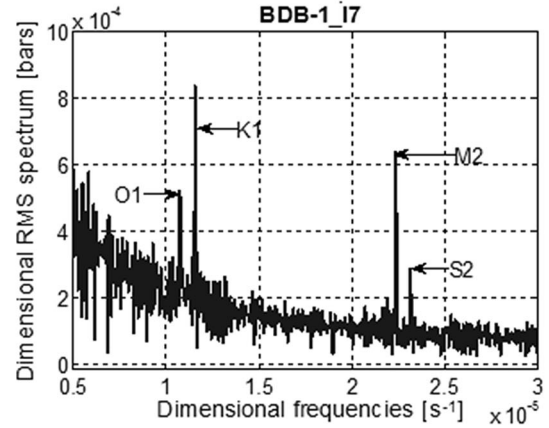
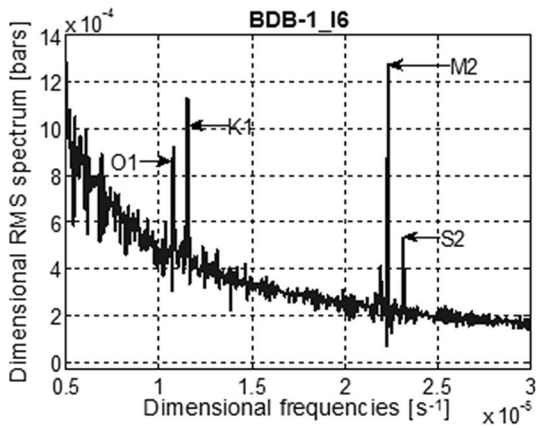
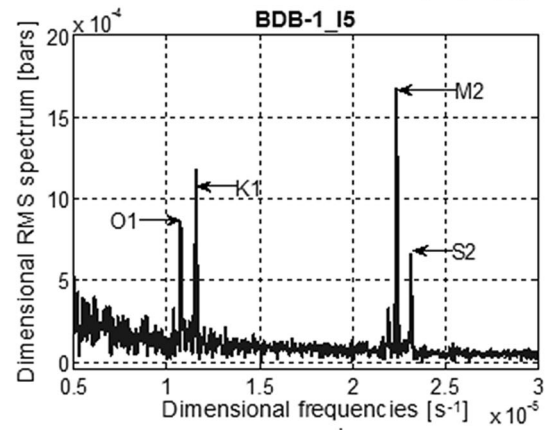
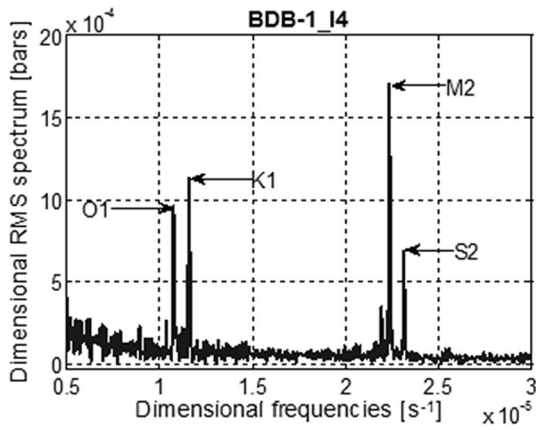
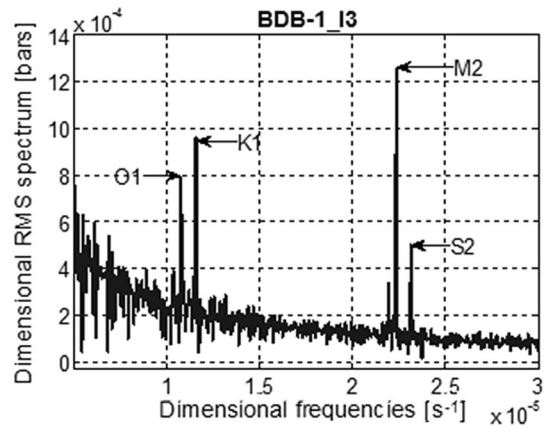
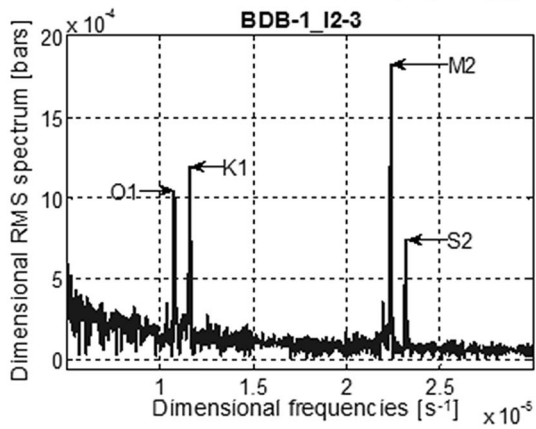
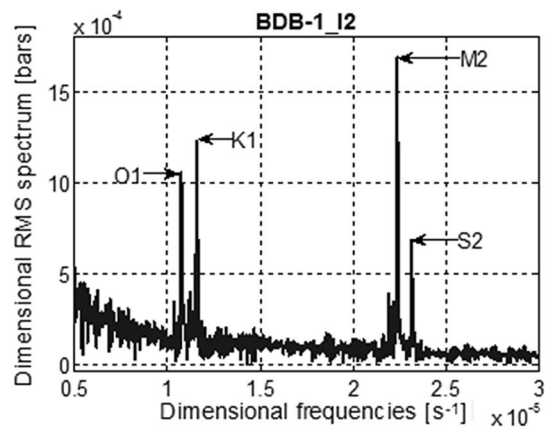
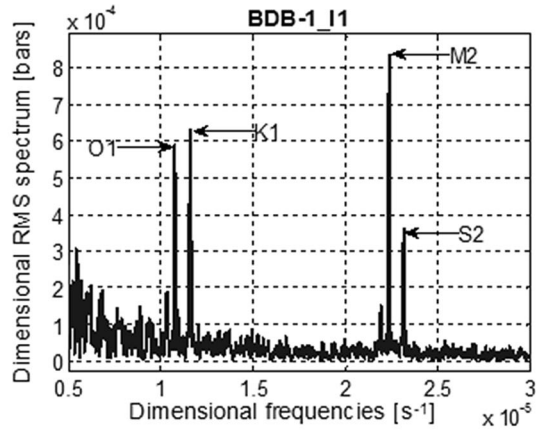


Table 4 Amplitudes of the tidal components with associated frequencies observed on BDB-1 pore pressure time series between 01/09/2014 and 10/03/2015

Formation/associated chamber	Amplitude on the RMS spectrum [bars]				Form ratio
	O ₁ (1.076 × 10 ⁻⁵ Hz)	K ₁ (1.161 × 10 ⁻⁵ Hz)	S ₂ (2.315 × 10 ⁻⁵ Hz)	M ₂ (2.236 × 10 ⁻⁵ Hz)	
Staffelegg formation/I ₁	5.886 × 10 ⁻⁴	6.326 × 10 ⁻⁴	3.606 × 10 ⁻⁴	8.353 × 10 ⁻⁴	1.02
OPA-shaly facies/I ₂	1.054 × 10 ⁻³	1.230 × 10 ⁻³	6.848 × 10 ⁻⁴	1.696 × 10 ⁻³	0.96
OPA-shaly facies/I ₂₋₃	1.041 × 10 ⁻³	1.192 × 10 ⁻³	7.390 × 10 ⁻⁴	1.823 × 10 ⁻³	0.87
OPA-carbonate-rich facies/I ₃	7.905 × 10 ⁻⁴	9.553 × 10 ⁻⁴	5.014 × 10 ⁻⁴	1.255 × 10 ⁻³	0.99
OPA-shaly facies/I ₄	9.560 × 10 ⁻⁴	1.133 × 10 ⁻³	6.838 × 10 ⁻⁴	1.701 × 10 ⁻³	0.88
OPA-shaly facies/I ₅	8.591 × 10 ⁻⁴	1.084 × 10 ⁻⁴	6.546 × 10 ⁻⁴	1.670 × 10 ⁻³	0.84
OPA-sandy facies/I ₆	8.637 × 10 ⁻⁴	1.205 × 10 ⁻³	5.329 × 10 ⁻⁴	1.278 × 10 ⁻³	1.04
Passwang formation/I ₇	5.200 × 10 ⁻⁴	7.206 × 10 ⁻⁴	2.825 × 10 ⁻⁴	6.360 × 10 ⁻⁴	1.35

Table 5 Specific storage coefficients (S_s) estimated from absolute pore pressure signals for BDB-1 borehole measuring intervals with corresponding formations and amplitudes of pressure head fluctuations Δh

Formation	Chamber	Δh [bar]	Δh [m]	S _s [m ⁻¹]
Upper toarcian-staffelegg formation	I ₁	8.353 × 10 ⁻⁴	8.52 × 10 ⁻³	2.4 × 10 ⁻⁶
Upper toarcian/lower aalenian-opalinus clay-shaly facies	I ₂	1.696 × 10 ⁻³	1.73 × 10 ⁻²	1.2 × 10 ⁻⁶
Upper toarcian/lower aalenian-opalinus clay-shaly facies	I ₂₋₃	1.823 × 10 ⁻³	1.86 × 10 ⁻²	1.1 × 10 ⁻⁶
Lower aalenian-opalinus clay-carbonate-rich facies	I ₃	1.255 × 10 ⁻³	1.28 × 10 ⁻²	1.6 × 10 ⁻⁶
Lower aalenian opalinus clay-shaly facies	I ₄	1.701 × 10 ⁻³	1.73 × 10 ⁻²	1.2 × 10 ⁻⁶
Middle aalenian-opalinus clay-shaly facies	I ₅	1.670 × 10 ⁻³	1.70 × 10 ⁻²	1.2 × 10 ⁻⁶
Upper aalenian-opalinus clay-sandy facies	I ₆	1.278 × 10 ⁻³	1.32 × 10 ⁻²	1.5 × 10 ⁻⁶
Upper aalenian-passwang formation	I ₇	6.360 × 10 ⁻⁴	6.49 × 10 ⁻³	3.1 × 10 ⁻⁶

Table 6 Spectral coherence function (Coh), arithmetic mean of the specific storativity coefficient (\tilde{S}_s), amplitude of the pore pressure signal 1 (A_{z1}), and of the pore pressure signal 2 (A_{z2}), vertical effective amplitude hydraulic conductivity (\tilde{K}_v^{Amp}) and vertical effective phase hydraulic conductivity ($\tilde{K}_v^{\Delta\varphi}$), effective dynamic porosity (ω) obtained for the M₂ earth tide for different couples of sensors in BDB-1 borehole

Chamber	Coh	\tilde{S}_s	A _{z1}	A _{z2}	Δφ	\tilde{K}_v^{Amp}	$\tilde{K}_v^{\Delta\varphi}$	B	ω	ω _{water loss}
	[-]	[m ⁻¹]	[bar]	[bar]	[rad]	[m s ⁻¹]	[m s ⁻¹]	[-]	[-]	[-]
I ₁ vs. I ₂	0.9985	1.8 × 10 ⁻⁶	8.35 × 10 ⁻⁴	1.70 × 10 ⁻³	-0.18220	4.7 × 10 ⁻⁸	7.2 × 10 ⁻⁷	0.2520	0.09	0.18
I ₂ vs. I ₂₋₃	0.9992	1.1 × 10 ⁻⁶	1.70 × 10 ⁻³	1.82 × 10 ⁻³	0.03573	2.5 × 10 ⁻⁶	1.0 × 10 ⁻⁵	1.0350	0.24	0.15
I ₂₋₃ vs. I ₃	0.9986	1.3 × 10 ⁻⁶	1.82 × 10 ⁻³	1.26 × 10 ⁻³	0.07658	1.4 × 10 ⁻⁷	3.3 × 10 ⁻⁶	0.3949	0.11	0.13
I ₃ vs. I ₄	0.9977	1.4 × 10 ⁻⁶	1.26 × 10 ⁻³	1.70 × 10 ⁻³	-0.06768	2.9 × 10 ⁻⁷	5.8 × 10 ⁻⁶	4.6810	1.33	0.12
I ₄ vs. I ₅	0.9930	1.2 × 10 ⁻⁶	1.70 × 10 ⁻³	1.67 × 10 ⁻³	0.02158	5.7 × 10 ⁻⁵	4.1 × 10 ⁻⁶	0.4758	0.12	0.14
I ₅ vs. I ₆	0.9965	1.4 × 10 ⁻⁶	1.67 × 10 ⁻³	1.28 × 10 ⁻³	-0.05037	6.4 × 10 ⁻⁷	1.8 × 10 ⁻⁵	0.2889	0.08	0.13
I ₆ vs. I ₇	0.9965	2.3 × 10 ⁻⁶	1.28 × 10 ⁻³	6.36 × 10 ⁻³	0.50810	3.9 × 10 ⁻⁸	7.3 × 10 ⁻⁸	1.6290	0.79	0.13

Mean water-loss porosity (ω_{water loss}) is given for comparison purposes

Shaded cells indicate spurious values

tests for the Opalinus Clay shaly facies: between 1×10^{-7} and $1 \times 10^{-4} \text{ m}^{-1}$, with a best estimate at $2 \times 10^{-6} \text{ m}^{-1}$ (Bossart and Thury 2008).

Effective dynamic porosity values obtained using the M₂ tide (Table 6) are globally in well agreement with those obtained from petrophysical measurements. Indeed,

coherent values between 8 and 24% are obtained by cross-analyses of measuring intervals located in the Opalinus Clay. Statistical analysis carried out in previous studies on Mont Terri samples (Fatmi 2009; Bailly and Matray 2015) revealed very low range values between 1 and 4% at the tunnel level. These unexplained low values could be

related to the hydraulically disturbed state of the studied area and desaturation phenomena.

Hydraulic conductivity values obtained in the saturated part of the claystone by cross-analysis (Table 6) are much higher than those obtained by other techniques. Indeed, high conductivities ranging between 5.7×10^{-5} and $1.4 \times 10^{-7} \text{ m s}^{-1}$ are found in the Opalinus Clay. These values are 6 to 8 orders of magnitude higher than the range expected from literature data, suggesting that the method is not appropriate for this formation. Discrepancies up to three orders of magnitude between laboratory hydraulic conductivity results and tidal analysis results were also reported by Boldt-Leppin and Hendry (2003) who studied the King site claystone formation (Canada). These discrepancies were explained by scale factor effects and the presence of fractured area.

Bailly and Matray (2015) performed statistical analysis on pore pressure time series acquired in the BCD-3 borehole located at the Mont Terri tunnel level. They obtained hydraulic conductivities ranging between 1.9×10^{-10} and $7.5 \times 10^{-11} \text{ m s}^{-1}$ in the unsaturated part of the Opalinus Clay by applying the same method on the S_1 solar diurnal tide. The M_2 tide was not found in the studied pore pressure time series due to suction conditions associated to the rock laboratory level. The study also suggested that the structures observed in this borehole were hydraulically conductive, meaning that the Opalinus Clay true permeability should be even lower than the range given by tidal analysis.

6 Discussion

6.1 Comparability of laboratory tests and in situ tests results

Reliable estimates of permeability and specific storage that describe the bulk hydraulic behaviour are needed for the evaluation of radionuclide transport in geological formations. Linking the results of laboratory tests to bulk characteristics at the regional scale is not straightforward and the meaning of measured values has to be interpreted. Sedimentary rocks are generally associated with anisotropic properties such as permeability, diffusion coefficient and mechanical features. In the Opalinus Clay, which is an overconsolidated clay, a moderate permeability anisotropy ratio of 5.5 was estimated based on laboratory permeameter tests (Muñoz et al. 2003; Croisé et al. 2004; Fernández-García et al. 2007).

The petrophysical model is based on a conceptual parallel plane geometry which would be associated to a flow orientation parallel to bedding planes. Since BDB-1 borehole was drilled perpendicular to bedding plane, the main solicited direction for fluid flow during hydraulic testing is

also parallel to stratification. For its part, tidal analysis is mainly based on gravitational forces that propagate radially from the center of the Earth and should result, given the setting of the Mont Terri anticline, in composite values of parallel and perpendicular to bedding permeabilities.

Although the petrophysical model may be unsuited to carbonated formations, calculation was also performed on the Passwang Formation and the Staffelegg Formation, which shows similar petrophysical parameters. Another questionable point is the use of a constant value for the Archie's exponent since this parameter depends on the nature of the porous medium. Consequently, adapted values should be taken in the future according to the evolution of rock facies along the stratigraphic sequence. Conductivities values obtained in BDB-1 with variable cementation factor (Fig. 12a) are only indicative and not quality-assured, given the uncertainties linked to data acquisition. Indeed, the Opalinus Clay was in the air-drilled section of the borehole, giving constraints for in situ determination of cementation factor.

Fitting the cementation factor by comparing petrophysical results and estimates from hydraulic tests can be debatable. Indeed, the volume of solicited rock is higher in the latter case and takes greater account of formation heterogeneities and local potentially open fractures. This point is clearly illustrated by the discrepancies observed for the Staffelegg Formation, in which many fractures were evidenced by drillcore mapping. Indeed, petrophysical measurements on centimetre-scale samples do not take into account these hydraulically conductive structures and underestimate the values of bulk properties.

Archie's law is rigorously an empirical relationship that links the electrical resistivity of saturated clay-free rocks and their porosity. However, an analogy can be made between the electrical potential and the concentration. It has been shown that effective diffusion coefficient could be predicted by this relationship in a variety of clays and shales with a cementation factor ranging between 2 and 3 (Boving and Grathwohl 2001; Van Loon et al. 2003; Mazurek et al. 2009). Best fit values of hydraulic conductivity obtained from hydraulic testing are generally higher than those computed with the petrophysical law (Fig. 12a). Hydraulic conductivities higher than $10^{-12} \text{ m s}^{-1}$ found in the Opalinus Clay shaly facies would be associated to illogical values of cementation factor inferior to 1.3, which was given for clean unconsolidated sand packs by Archie (1942).

Whether it be for pulse or constant withdrawal tests, the numerical interpretation of hydraulic tests suggests rather wide and unrealistic ranges of uncertainties for hydraulic conductivity and specific storage. Covering several orders of magnitude and not tightly around the best estimates (Table 3), these uncertainties are probably linked to the

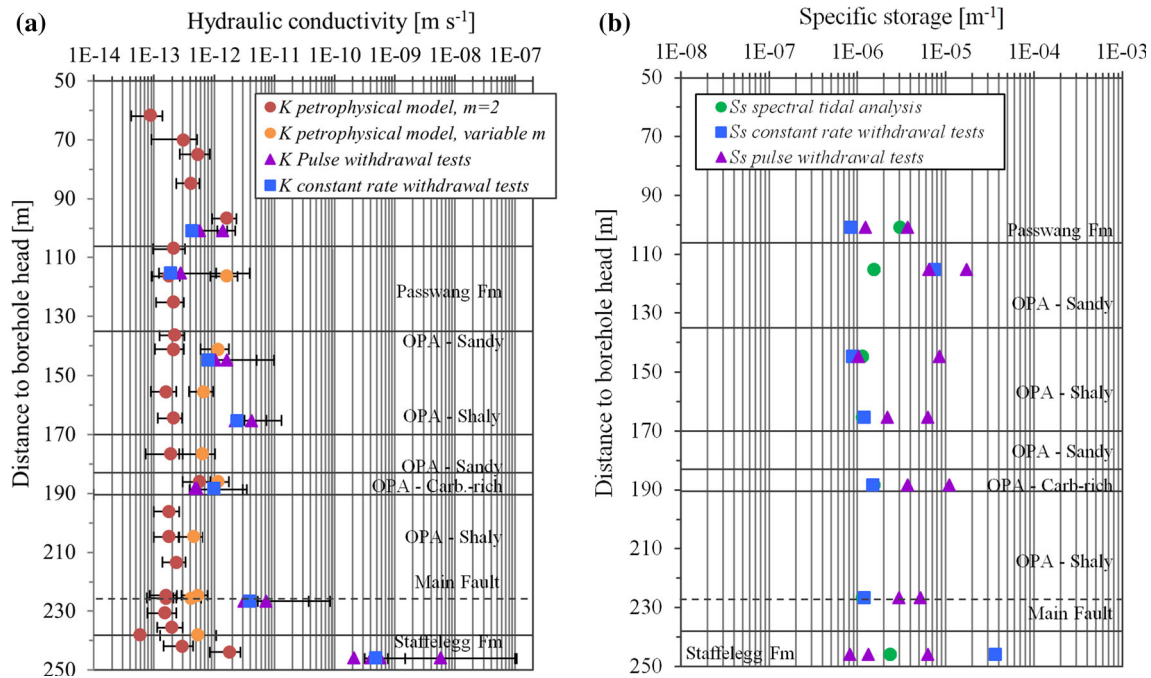


Fig. 12 Comparison of results obtained by petrophysical analysis, in situ hydraulic testing and tidal spectral analysis performed on BDB-1 borehole: **a** hydraulic conductivity **b** specific storage

large number of fitted parameters. Tidal analysis may be more representative than single well hydraulic testing for specific storage estimation (Fig. 12b), since the tidal deformation is applied to the entire rockmass. The highest values for specific storage obtained from pulse testing should be taken with caution since the sensitivity to this parameter is low for this kind of test (Cooper et al. 1967).

6.2 Consistency with previous results

Numerous in situ and laboratory investigations have been carried out at the Mont Terri rock laboratory to characterize the hydraulic properties of the Opalinus Clay. Laboratory permeameter tests revealed conductivity values ranging from 6 to $12 \times 10^{-14} \text{ m s}^{-1}$ with high associated storage coefficient of $4.8 \times 10^{-4} \text{ m}^{-1}$ (Croisé et al. 2004). Figure 13 shows a compilation of hydraulic conductivity results obtained from packer tests (pulse, constant head and constant rate) performed previously at the Mont Terri site (Lavanchy and Mettier 2012), along with data collected in BDB-1 borehole. Tests were mainly performed in boreholes oblique or normal to bedding drilled in area unaffected by the excavation damaged zone of the tunnel. Previous permeability values measured at the rock laboratory level range from 1.5×10^{-14} to $1.1 \times 10^{-9} \text{ m s}^{-1}$ with 55% of the values in the order of $10^{-13} \text{ m s}^{-1}$. The high values above $1.1 \times 10^{-10} \text{ m s}^{-1}$ of the shaly facies from previous studies might be affected by the excavation

damaged zone (EDZ) and are not quality assured. The best fit values obtained from BDB-1 hydraulic testing fall virtually in the expected range with higher values in the order of $10^{-12} \text{ m s}^{-1}$ characterising the Opalinus Clay shaly facies.

Specific storage coefficients obtained by tidal analysis are rather homogeneous within the Opalinus Clay with values in the order of 10^{-6} m^{-1} , which are comparable to the range of 2×10^{-6} to $5 \times 10^{-6} \text{ m}^{-1}$ found by Bailly and Matray (2015).

No significant correlation between the hydraulic conductivity and the different lithological facies was highlighted by Croisé et al. (2004), Nussbaum and Bossart (2004) and Lavanchy and Mettier (2012) due to a lack of data from the sandy facies. Although best fit values obtained from BDB-1 borehole indicate higher values in the shaly facies, uncertainty ranges make it difficult to conclude on a possible contrast. Numerical simulations show that sandstone lenses embedded in clay rich strata do not compromise the barrier function of the Opalinus Clay since low hydraulic conductivity values characterise the entire formation. Furthermore, Opalinus Clay sandy layers are better cemented and display lower porosities (Fig. 5a). Microscopic observations in the sandy facies revealed precipitation of authigenic quartz, carbonates and kaolinite (Peters et al. 2011). On the other hand, porosity values measured in BDB-1 borehole are globally lower than those obtained at the rock laboratory tunnel level and may reflect

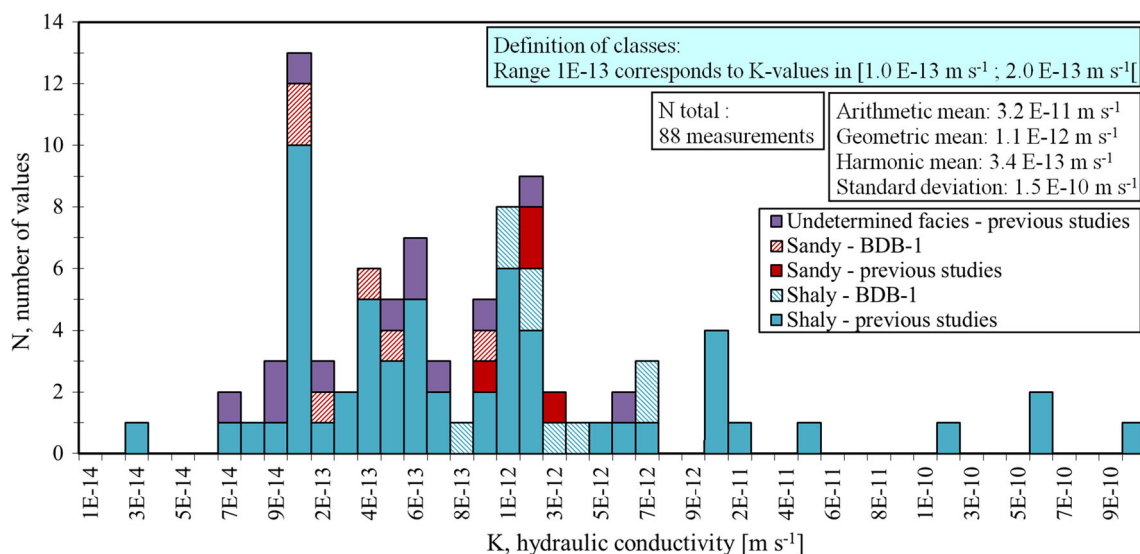


Fig. 13 Compilation of results from hydraulic borehole packer tests performed on the Opalinus Clay at the Mont Terri rock laboratory. The high values of the shaly facies from previous studies might be

the deconfinement and relaxation of stresses occurring at the latter location.

The Main Fault that intersects the laboratory does not impact the barrier function of the Opalinus Clay. Indeed, the sealing of fault planes by calcite shear fibres and clay minerals induce small effect of tectonic deformation on the hydraulic properties of the Opalinus Clay (Nussbaum et al. 2011). This observation is supported by the consistency between the hydraulic tests performed in the intact shaly facies and those carried out in the interval crossing the fault zone. Similarly, no contrast can be identified on the different profiles obtained with the petrophysical model.

7 Conclusions

The deep borehole (DB) experiment enabled the acquisition of data in a fresh borehole penetrating the entire hydraulically undisturbed Opalinus Clay at Mont Terri. Therefore, the presented results are unique, because other hydraulic data at Mont Terri are or might be influenced by tunneling and experimental activities. Three methods with different investigation volumes were carried out and compared.

A model that links intrinsic permeability to petrophysical parameters gives intrinsic permeability values ranging between 2×10^{-21} and 6×10^{-20} m² for a cementation factor varying between 2 and 3, corresponding to hydraulic conductivities between 2×10^{-14} and 6×10^{-13} m s⁻¹. Tidal analysis revealed itself not to be an appropriate method to compute hydraulic conductivity in our study, giving values overestimated of several orders of

affected by the EDZ and are not quality assured (modified from Lavanchy and Mettier 2012)

magnitudes. However, this approach gives reasonable values for specific storage and effective porosity. As a third method, in situ hydraulic testing was performed using the multipacker system installed in BDB-1 borehole. Hydraulic conductivity values obtained by numerical inversion from pulse tests are consistent with those deduced from constant rate withdrawal tests, and suggest a slight vertical variability across the formation in the range of 1×10^{-13} to 7×10^{-12} m s⁻¹, possibly due to local variations of the matrix structure, composition and cementation, or the presence of fractures. In conclusion, the hydraulic conductivity values of the deep borehole (DB) experiment agree well with previous hydraulic testing results performed in the hydraulically disturbed Opalinus Clay around the Mont Terri rock laboratory. Therefore, future hydraulic testing in the laboratory outside the excavated damaged zone can be rated as comparable to undisturbed conditions. However, results obtained in BDB-1 borehole show higher values (in the order of 10^{-12} m s⁻¹) for the Opalinus Clay shaly facies than its sandy facies (in the order of 10^{-13} m s⁻¹), which is consistent with previous microscopic observations (Peters et al. 2011). Further laboratory experiments using Hassler cells will be performed to characterise the Opalinus Clay permeability anisotropy in the future.

Petrophysical analysis of drillcores and time-series analyses are complementary to hydraulic testing. These techniques involve different volumes of investigation. Core analysis, as well as laboratory permeameter tests, give the homogeneous matrix hydraulic properties but do not account for larger scale heterogeneities such as sedimentary and tectonic features. Moreover, analyses on core

samples might be influenced by deconfining and alteration of the core material, thus resulting in biased values. Therefore, hydraulic testing in a fresh borehole is the recommended method for determination of hydraulic conductivity in overconsolidated clays. However, the pressure perturbations e.g., induced by drilling activities have to be taken into account for design and analyses of hydraulic testing. The dissipation of drilling and installation of instrumentation induced pressure perturbations can be identified by the tidal components in the pore pressure time series. Our study showed that drilling the BDB-1 borehole with air as drilling fluid and a saturation with artificial pore-water was an appropriate choice for our application, because: (1) no mud-cake was created, (2) no artificial osmotic effects and borehole convergence were observed so far, (3) future water sampling can be carried out since there was no contamination with drilling mud, and (4) we reached fully undisturbed formation pressures after several months. The latter was possible to do so in an underground laboratory experiment, due no time and financial constraints, which are limiting factors on drill site for exploration boreholes. Therefore, in clay formations, particular care should be taken in the choice of drilling method and drilling fluid as well as borehole instrumentation materials, in order to obtain accurate hydraulic parameters.

Acknowledgements This study was performed in the framework of the deep borehole (DB) experiment, financed by six partners of the International Mont Terri Consortium (swisstopo, NAGRA, BGR, GRS, NWMO, IRSN). The authors would like to thank Karam Kontar and Jocelyn Gisiger (Solexperts AG) for their technical support and realisation of hydraulic testing, as well as Christelle Courbet (IRSN) and Benoît Paris (INTERA) for advices on numerical interpretation. The MuStat v1 package used in this paper is the result of previous works respectively done by: Alain Mangin (CNRS, Laboratoire d'écologie des hydrosystèmes de Moulis), David Labat (Géosciences Environnement Toulouse), Rachid Ababou (CNRS/INPT/IMFT), Hassane Fatmi (PhD at IRSN and CNRS/INPT/IMFT) and David Bailly (TREES Institute). The constructive and careful reviews of Prof. Z. Jiang (Queensland University of Technology, Brisbane, Australia) and Prof. P. Cosenza (University of Poitiers, France) contributed to improve the initial version of this article and are greatly acknowledged.

Open Access This article is distributed under the terms of the Creative Commons Attribution 4.0 International License (<http://creativecommons.org/licenses/by/4.0/>), which permits unrestricted use, distribution, and reproduction in any medium, provided you give appropriate credit to the original author(s) and the source, provide a link to the Creative Commons license, and indicate if changes were made.

References

- Ababou, R., Fatmi, H., Matray, J. M., Nussbaum, C., & Bailly, D. (2012). Statistical analyses of pore pressure signals in claystone during excavation works at the Mont Terri Underground Research Laboratory. In R. Abdel Rahman (Ed.), *Radioactive waste* (pp. 373–430). Publisher: InTech.
- Altinier, M. V. (2006). Etude de la composition isotopique des eaux porales de l'argilite de Tournemire : intercomparaison des méthodes de mesure et relations avec les paramètres pétrophysiques. Ph. D. dissertation, Université Paris-Sud, Orsay, France, pp. 200
- Archie, G. E. (1942). The electrical resistivity log as an aid in determining some reservoir characteristics. *Transactions of the American Institute of Mining Metallurgical, and Petroleum Engineers*, 146, 54–62.
- Bailly, D., Matray, J. M., & Ababou, R. (2014). Temporal behavior of a ventilated claystone at the Tournemire URL: Cross-spectral analyses focused on daily harmonics. *Engineering Geology*, 183, 137–158.
- Bailly, D., & Matray, J.-M. (2015). LP-A Experiment: Phase 20, Statistical analysis of time series acquired in the EZ-B Niche and at the Main fault. Mont Terri Technical Note, TN 2014-59, 79 pp. Federal Office of Topography (swisstopo), Wabern, Switzerland. www.mont-terri.ch.
- Barker, J. A. (1988). A generalized radial-flow model for hydraulic tests in fractured rock. *Water Resources Research*, 24(10), 1796–1804.
- Beauheim, R. L., Roberts, R. M., & Avis, J. D. (2004). Well testing in fractured media: flow dimensions and diagnostic plots. *Journal of Hydraulic Research*, 42, 69–76.
- Beauheim, R. L., & Roberts, R. M. (2004). Well-test analysis techniques developed for the Waste Isolation Pilot Plant. In Proceedings of the 66th EAGE Conference and Exhibition, Paris, France.
- Blaesi, H.-R., Peters, T. J., & Mazurek, M. (1991). Der Opalinus-Ton des Mt. Terri (Kanton Jura): Lithologie, Mineralogie und physiko-chemische Gesteinsparameter. Nagra Interner Bericht, (pp. 90–60). Nagra, Wettingen, Switzerland. www.nagra.ch.
- Boldt-Leppin, B. E. J., & Hendry, J. (2003). Application of Harmonic Analysis of Water Levels to Determine Vertical Hydraulic Conductivities in Clay-Rich Aquitards. *Ground Water*, 41(4), 514–522.
- Bossart, P., & Thury, M. (2008). Mont Terri Rock Laboratory. Project, Programme 1996 to 2007 and Results. Reports of the Swiss Geological Survey, No. 3, p 445. Federal Office of Topography (swisstopo), Wabern, Switzerland. www.mont-terri.ch.
- Bossart, P., Bernier, F., Birkholzer, J., Bruggeman, C., Connolly, P., Dewonck, S., Fukaya, M., Herfort, M., Jensen, M., Matray, J.-M., Mayor, J. C., Moeri, A., Oyama, T., Schuster, K., Shigeta, N., Vietor, T., & Wieczorek, K. (2017). Mont Terrirock laboratory, 20 years of research: introduction, site characteristics and overview of experiments. *Swiss Journal of Geosciences*, 110. doi:10.1007/s00015-016-0236-1 (this issue).
- Boulin, P. F., Bretonnier, P., Gland, N., & Lombard, J. M. (2012). Contribution of the steady state method to water permeability measurement in very low permeability porous media. *Oil and Gas Science and Technology*, 67, 387–401.
- Boving, T. B., & Grathwohl, P. (2001). Tracer diffusion coefficients in sedimentary rocks: correlation between porosity and hydraulic conductivity. *Journal of Contaminant Hydrogeology*, 53(1), 85–100.
- Bredehoeft, J. D. (1967). Response of well-aquifer systems to Earth tides. *Journal of Geophysical Research*, 72(12), 3075–3087.
- Bredehoeft, J. D., & Papadopoulos, S. S. (1980). A method for determining the hydraulic properties of tight formations. *Water Resources Research*, 16(1), 233–238.
- Butler, J. J. (1998). *The design and performance, and analysis of slug tests* (p. 252). Boca Raton: Lewis Publishers (imprint of CRC Press LLC).

- Chapuis, R. P., & Aubertin, M. (2003). *Predicting the Coefficient of Permeability of Soils Using the Kozeny-Carman Equation* (p. 35). Montréal: Ecole Polytechnique de Montréal.
- Clauer, N., Techer, I., Nussbaum, C., & Laurich, B. (2017). Geochemical signature of paleofluids in microstructures from “Main Fault” in the Opalinus Clay of the Mont Terri rock laboratory, Switzerland. *Swiss Journal of Geosciences*, 110. doi:10.1007/s00015-016-0253-0 (this issue).
- Cooper, H. H., Bredehoeft, J. D., & Papadopoulos, I. S. (1967). Response of a finite-diameter well to an instantaneous charge of water. *Water Resource Research*, 3, 263–269.
- Croisé, J., Schilckenrieder, L., Marschall, P., Boisson, J. Y., Vogel, P., & Yamamoto, S. (2004). Hydrogeological investigations in a low permeability claystone formation: the Mont Terri Rock Laboratory. *Physics and Chemistry of the Earth*, 29, 3–15.
- Cuttillo, P. A., & Bredehoeft, J. D. (2011). Estimating aquifer properties from the water level response to earth tides. *Ground Water*, 49(4), 600–610.
- Doodson A. T., & Warburg, H. D. (1941). Admiralty manual of tides. Her Majesty’s Stationary Office, London, xii, p 270.
- Fatmi, H. (2009). *Méthodologie d’analyse des signaux et caractérisation hydrogéologique: application aux chroniques de données obtenues aux laboratoires souterrains du Mont Terri, Tournemire et Meuse/Haute-Marne*. Ph.D. dissertation (p. 249). Toulouse: Université de Toulouse.
- Fatmi, H., Ababou, R., & Matray, J.-M. (2008). Statistical pre-processing analyses of hydrometeorological time series in a geological clay site (methodology and first results for Mont Terri’s PP experiment). *Journal of Physical Chemistry Letters A/B/C*, 33, S14–S23.
- Fernández-García, D., Gómez-Hernández, J. J., & Mayor, J. C. (2007). Estimating hydraulic conductivity of the Opalinus Clay at the regional scale: Combined effect of desaturation and EDZ. *Physics and Chemistry of the Earth, Parts A/B/C*, 32(8), 639–645.
- Fierz, T., & Rösli, U. (2014). Mont Terri DB Experiment: Installation of a 7-interval multi-packer system into borehole BDB-1. Instrumentation Report. Mont Terri Technical Note, TN 2014-23. p 37. Federal Office of Topography (swisstopo), Wabern, Switzerland. www.mont-terri.ch.
- Gautschi, A. (2001). Hydrogeology of a fractured shale (Opalinus Clay): Implications for the deep disposal of radioactive wastes. *Hydrogeology Journal*, 9, 97–107.
- Horseman, S. T., Higgo, J. J. W., Alexander, J., & Harrington, J. F. (1996). Water, Gas and Solute Movement Through Argillaceous Media. Nuclear Energy Agency Rep., CC-96/1, OECD, Paris, p 306.
- Hostettler, B., Reisdorf, A. G., Jaeggi, D., Deplazes, G., Bläsi, H.-R., Morard, A., Feist-Burkhardt, S., Waltschew, A., Dietze, V., & Menkveld-Gfeller, U. (2017). Litho- and biostratigraphy of the Opalinus Clay and bounding formations in the Mont Terri rock laboratory (Switzerland). *Swiss Journal of Geosciences*, 110. doi:10.1007/s00015-016-0250-3 (this issue).
- Jiang, Z., Martiethoz, G., Taulis, M., & Cox, M. (2013). Determination of vertical hydraulic conductivity of aquitards in a multi-layered leaky system using water-level signals in adjacent aquifers. *Journal of Hydrology*, 500, 170–182.
- Johns, R. T., Vomvoris, S. G., & Löw, S. (1995). *Review of hydraulic field tests in the Opalinus Clay of Northern Switzerland*. Nuclear Energy Agency: Hydraulic and hydrochemical characterisation of argillaceous rocks.
- Kell, G. S. (1975). Volume properties of ordinary water. In R. C. Weast (Ed.), *Handbook of chemistry and physics* (56th ed.). Cleveland: CRC Press.
- Keller, C. K., Van der Kamp, G., & Cherry, J. A. (1989). A multiscale study of the permeability of a thick clayey till. *Water Resources Research*, 25(11), 2299–2317.
- Kostek, S., Schwartz, L., & Johnson, D. (1992). Fluid permeability in porous media: Comparison of electrical estimates with hydrodynamical calculations. *Physical Review B*, 45(1), 186–194.
- Lavanchy, J. M., & Mettier, R. (2012). HA (Hydrogeological analysis) Experiment: Hydraulic database, Phases 1-16, Version 1.0. Mont Terri Technical Note, TN 2010-74, p 22. Federal Office of Topography (swisstopo), Wabern, Switzerland. www.mont-terri.ch.
- Marschall, P., Horseman, S., & Gimmi, T. (2005). Characterisation of gas transport properties of the Opalinus Clay, a potential host rock formation for radioactive waste disposal. *Oil and Gas Science and Technology*, 60(1), 121–139.
- Matray, J.-M., Savoye, S., & Cabrera, J. (2007). Desaturation and structure relationships around drifts excavated in the well-compacted Tournemire’s argillite (Aveyron, France). *Engineering Geology*, 90, 1–16.
- Mazurek, M., Hurford, A., & Leu, W. (2006). Unravelling the multi-stage burial history of the Swiss Molasse Basin: integration of apatite fission track, vitrinite reflectance and biomarker isomerisation analysis. *Basin Research*, 18, 27–50.
- Mazurek, M., Alt-Epping, P., Bath, A., Gimmi, T., & Waber, H. N. (2009). *Natural tracer profiles across argillaceous formations: The CLAYTRAC Project* (p. 365). Paris: Nuclear Energy Agency report, OECD.
- Mejías, M., Renard, P., & Glenz, D. (2009). Hydraulic 652 testing of low-permeability formations: A case study in the granite of Cadalso de los Vidrios, Spain. *Engineering Geology*, 107, 88–107.
- Melchior, P. (1978). *The tides of the planet Earth* (p. 609). Oxford: Pergamon Press.
- Mercer, J. W., Pinder, G. F., & Donalson, I. G. (1975). A Galerkin-finite element analysis of the hydrothermal system at Wairakei, New-Zealand. *Journal of Geophysical Research*, 80, 2608–2621.
- Merritt, M. L. (2004). Estimating hydraulic properties of the Floridan aquifer system by analysis of earth-tide, ocean-tide, and barometric effects. Collier and Hendry Counties, Florida. U.S. Geological Survey Water-resources investigations Report 03-4267, p 70.
- Monnier, G., Stengel, P., & Fies, J. C. (1973). Une méthode de mesure de la densité apparente de petits agglomérats terreux. Application à l’analyse de système de porosité du sol. *Annales Agronomiques*, 24, 533–545.
- Muñoz, J. J., Lloret, A., & Alonso, E. (2003). Laboratory Report: Characterization of hydraulic properties under saturated and non saturated conditions. Project Deliverable, 4.
- Nagra (2002). Projekt Opalinuston: Konzept für die Anlage und den Betrieb eines geologischen Tiefenlagers: Entsorgungsnachweis für abgebrannte Brennelemente, verglaste hochaktive sowie langlebige mittelaktive Abfälle. Nagra Technical Report, 02-02, p 24. Nagra, Wettingen, Switzerland. www.nagra.ch.
- Neuzil, C. E. (1982). On conducting the modified ‘slug’ test in tight formations. *Water Resources Research*, 18(2), 439–441.
- Neuzil, C. E. (1994). How permeable are clays and shales? *Water Resources Research*, 30(2), 145–150.
- Neuzil, C. E. (2000). Osmotic generation of “anomalous” fluid pressures in geological environments. *Nature*, 403, 182–184.
- Nussbaum, C., & Bossart, P. (2004). Compilation of K-values from packer tests in the Mont Terri rock laboratory. Mont Terri Technical Note, TN 2005-10, p 29. Federal Office of Topography (swisstopo), Wabern, Switzerland.
- Nussbaum, C., Bossart, P., Amann, F., & Aubourg, C. (2011). Analysis of tectonic structures and excavation induced fractures in the Opalinus Clay, Mont Terri underground rock laboratory (Switzerland). *Swiss Journal of Geosciences*, 104, 187–210.
- Nussbaum, C., Kloppenburg, A., Caer, T. & Bossart, P. (2017). Tectonic evolution of the Mont Terri anticline based on forward

- modelling. *Swiss Journal of Geosciences*, 110. doi:10.1007/s00015-016-0248-x (this issue).
- Pape, H., Clauser, C., & Iffland, J. (1999). Permeability prediction based on fractal pore-space geometry. *Geophysics*, 64, 1447–1460.
- Pearson, F. J., Arcos, D., Boisson, J-Y., Fernández, A. M., Gäbler, H.E., Gaucher, E., Gautschi, A., Griffault, L., Hernán, P., & Waber, N. (2003). Mont Terri Project-Geochemistry of water in the Opalinus Clay Formation at the Mont Terri Rock Laboratory. Reports of the Swiss Geological Survey, No. 5, p 143. Federal Office of Topography (swisstopo), Wabern, Switzerland. www.mont-terri.ch.
- Peters, M., Mazurek, M., Jaeggi, D., & Müller, H. (2011). WS-H Experiment: Heterogeneities in the sandy facies of Opalinus Clay on a scale on millimetres to centimeters. Mont Terri Technical Note, TN 2010-76, p 66. Federal Office of Topography (swisstopo), Wabern, Switzerland.
- Terzaghi, V. K. (1936). The shearing resistance of saturated soils and the angle between the planes of shear. *First International Conference of Soil Mechanics*, Harvard University Press, 1, 54–56.
- Timms, W. A., & Acworth, R. I. (2005). Propagation of pressure change through thick clay sequences: an example from Liverpool Plains, NSW, Australia. *Hydrogeology Journal*, 13(5–6), 858–870.
- Tremosa, J. (2010). Influence of osmotic processes on the excess-hydraulic head measured in the Toarcian/Domerian argillaceous formation of Tournemire. Ph.D. dissertation (p. 322). Paris: Université Pierre et Marie Curie.
- UNESCO. (1981). Tenth report on the joint panel on oceanographic tables and standard. *UNESCO Technical Paper in Marine Science*, 36, 28.
- Ullman, W. J., & Aller, R. C. (1982). Diffusion coefficients in nearshore marine sediments. *Limnology and Oceanography*, 27, 552–556.
- Van Loon, L. R., & Mibus, J. (2015). A modified version of Archie's law to estimate effective diffusion coefficients of radionuclides in argillaceous rocks and its application in safety analysis studies. *Applied Geochemistry*, 59, 85–94.
- Van Loon, L. R., Soler, J. M., Jakob, A., & Bradbury, M. H. (2003). Effect of confining pressure on the diffusion of HTO, $^{36}\text{Cl}^-$ and $^{125}\text{I}^-$ in a layered argillaceous rock (Opalinus Clay): diffusion perpendicular to the fabric. *Applied Geochemistry*, 18, 1653–1662.
- Van der Kamp, G. (2001). Methods for determining the in situ hydraulic conductivity of shallow aquitards—an overview. *Hydrogeology Journal*, 9, 5–16.
- Wiegel, R. L. (1964). *Tsunamis, storm surges, and harbour oscillations*. In *Oceanographical Engineering* (pp. 95–127). Englewood Cliffs: Prentice Hall.
- Yu, L., Rogiers, B., Gedeon, M., Marivoet, J., Craen, M. D., & Mallants, D. (2013). A critical review of laboratory and in situ hydraulic conductivity measurements for the Boom Clay in Belgium. *Applied Clay Science*, 75, 1–12.